

Layer Collapse Can be Induced by Unstructured Pruning

Zhu Liao

LTCI, Télécom Paris, Institut Polytechnique de Paris

zhu.liao@telecom-paris.fr

Victor Quéту

LTCI, Télécom Paris, Institut Polytechnique de Paris

victor.quetu@telecom-paris.fr

Van-Tam Nguyen

LTCI, Télécom Paris, Institut Polytechnique de Paris

van-tam.nguyen@telecom-paris.fr

Enzo Tartaglione

LTCI, Télécom Paris, Institut Polytechnique de Paris

enzo.tartaglione@telecom-paris.fr

Abstract

Unstructured pruning is a popular compression method for efficiently reducing model parameters. However, while it effectively decreases the number of parameters, it is commonly believed that unstructured pruning cannot shorten the computational critical path, i.e., the maximum number of layers traversed during forward propagation.

In this paper, we study when and how unstructured pruning can yield structural effects. For rectifier-activated networks, we introduce the notion of neuron entropy, which quantifies the degree of nonlinearity utilization. We show that magnitude-based pruning naturally lowers this entropy, sometimes down to zero-entropy layers that become linearizable and can thus be removed. Building on this insight, we propose a method that leverages "unstructured" pruning to favor sparsity in low-entropy layers, enabling their complete removal. We validate the phenomenon across CNNs, Vision Transformers, and NLP models: unstructured pruning can induce effective layer removal with little or no performance degradation in over-parameterized networks. Our code is available at <https://github.com/ZhuLIA0001/NEPENTHE.git>.

1 Introduction

Artificial Intelligence has undergone a transformative evolution propelled by the advent of Deep Neural Networks (DNNs), which have emerged as instrumental in achieving state-of-the-art outcomes across pivotal computer vision domains, including semantic segmentation (Lu et al., 2022) and classification (Zhang et al., 2023; Arslan et al., 2022). Notably, the pervasive impact of DNNs extends beyond conventional computer vision tasks, showcasing absolute potential in realms such as natural language processing (Touvron et al., 2023), and multi-modal tasks (Sun et al., 2018).

While DNNs' performance has exhibited scalability concerning model and dataset size (Hestness et al., 2017), the inherent computational burden is one major downside. Notably, contemporary state-of-the-art models are characterized by millions (or even billions) of parameters, demanding billions (or trillions) of floating-point operations (FLOPs) for a single input prediction (Guo et al., 2022). The heavy hardware and energy demands of large networks hinder real-time and edge applications.

Over the past decade, the research landscape has witnessed the emergence of compression techniques as a crucial avenue to address the resource-intensive nature of DNNs. Intrinsically, there exists a link between the generalization capability of DNNs and the model's complexity: off-the-shelf architectures employed in downstream tasks are, in many cases, over-parametrized, representing a threat for generalization (Hestness et al., 2017). Removing redundant parameters improves both computation and generalization (Tartaglione

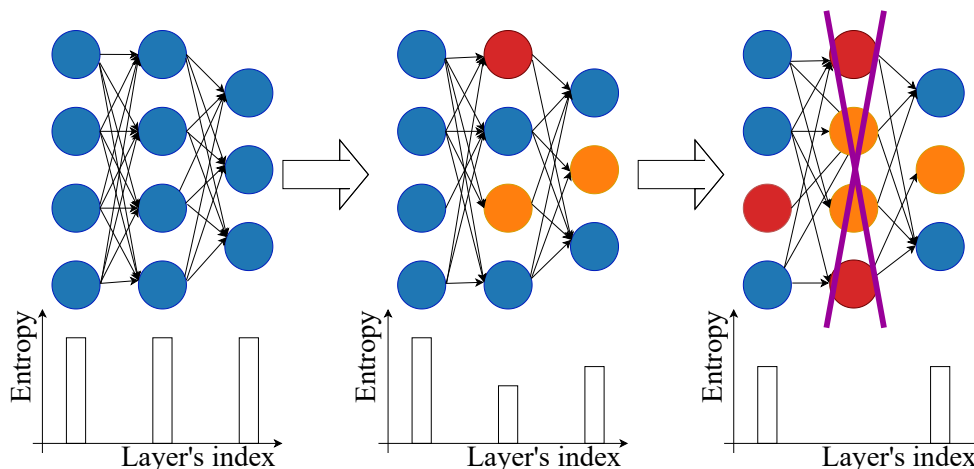


Figure 1: In this work, we show that the average neuron’s entropy calculated at the layer scale reduces as we induce some sparsity in the model, and once it reaches zero, the layer becomes linearizable and thus can be removed.

et al., 2021; 2022). Recently, the most widely used compression technique that removes the greatest number of parameters is unstructured pruning (Han et al., 2015), which eliminates individual weights based on their magnitude without considering the network’s structure.

Nevertheless, the impact of removing individual parameters or whole filters on recent computing resources, such as GPUs, is relatively marginal. Due to the parallelization of computations, the size of layers, whether larger or smaller, is primarily constrained by memory caching and core availability. The bottleneck in computation lies in the *critical path* that forward-propagation must traverse (Ali Mehmeti-Göpel & Disselhoff, 2023), a challenge that can be addressed by strategically removing layers.

It is commonly believed that unstructured pruning can only remove parameters but not shorten network depth. However, our theoretical and experimental evidence demonstrates that this perception is incomplete: unstructured pruning can induce layer collapse. In rectifier-activated networks, unstructured pruning reduces the neuron entropy and when a layer’s average entropy drops to zero, the layer becomes linearizable and can be removed. Therefore, we design an unstructured entropy-weighted allocation pruning scheme aimed at driving the entropy value of the low-entropy layer to zero with minimal performance loss. We summarize, here below, our key messages and contributions.

- We propose an entropy measure at the single-neuron level, indicating how much a neuron relies on its linear component. By minimizing this entropy, the neuron can be effectively linearized, and when the average entropy across neurons approaches zero, the layer itself becomes entirely linear (Sec. 3.1).
- We theoretically show that “unstructured” pruning, in rectifier-activated layers, naturally reduces the layer’s entropy (Sec. 3.2), and further demonstrate it empirically (Sec. 4.2).
- We propose NEPENTHE, a novel method that reduces a neural network’s effective depth (Sec. 3.3) by performing an entropy-guided reallocation of the unstructured pruning budget across layers (Sec. 3.3), and validate its effectiveness across a variety of setups and popular architectures (Sec. 4.3).

2 Related Works

Neural Network Pruning. Neural network pruning attracts attention for improving efficiency and reducing overfitting. Its goal is to reduce a cumbersome network to a smaller one while maintaining accuracy by removing irrelevant weights, filters, or other structures from neural networks. While *structured* pruning removes entire neurons, filters, or channels (Tartaglione et al., 2021; He & Xiao, 2023; Lin et al., 2020),

unstructured pruning algorithms remove weights without explicitly considering the neural network’s structure (Han et al., 2015). Magnitude-based pruning, where the importance score to prune parameters is based on their magnitude (Han et al., 2015; Louizos et al., 2018; Zhu & Gupta, 2017), and gradient-based pruning, where the ranking or the penalty term is a function of the gradient magnitude (or to higher order derivatives) (Lee et al., 2019; Tartaglione et al., 2022), are the main types of unstructured pruning approaches. Blalock et al. (2020) compared the effectiveness of these approaches and concluded that, in general, gradient-based methods are less accurate than magnitude-based methods. Moreover, Gale et al. (2019) showed that simple magnitude pruning approaches achieve comparable or better results than complex methods, making them a good trade-off between complexity and competitiveness. In addition to magnitude-based pruning, a recent method called Wanda (Sun et al., 2024) ranks each weight by the absolute product of its magnitude and its input feature, pruning those with the lowest scores. We verify that the phenomenon discussed in this paper also holds for Wanda, showing its generality across different pruning criteria. From a computational perspective, it is widely recognized that structured pruning offers greater advantages over unstructured methods in general-purpose hardware environments, both in terms of memory and computation, despite achieving significantly lower sparsity levels (Bragagnolo et al., 2021). In this work, we focus on bridging this gap: investigating when and how unstructured pruning can induce structural effects.

Entropy-Guided Pruning. Some works have already tried to propose entropy-based approaches to guide pruning. For convolutional neural networks, Luo & Wu (2017) put forward an iterative filter pruning strategy in which the importance of each filter is calculated by its entropy-based channel selection metric. To recover performance, the pruned model is then fine-tuned. Also for CNNs, Hur & Kang (2019) suggested an entropy-based method that determines dynamically during training the threshold by considering the average amount of information from the weights to the output. Moreover, Min et al. (2018) proposed a two-stage filter pruning framework, first intra-layer and then extra-layer. Given that the entropy is a measure of disorder, evidently, it identifies filters that mutually have low entropy: these can be considered redundant and can be removed from the model. These methods reduce width, not depth. EASIER (Quéru et al., 2024) proposed an entropy-based importance metric to collapse low-information layers and reduce network depth. By measuring per-layer neuron entropy, they identify layers whose activations lie almost entirely in a linear or inactive regime and remove them wholesale. Although this approach relies on an entropy-based metric, it performs structured layer removal rather than applying unstructured weight pruning to directly lower entropy values. Similarly, recent work (Lin et al., 2024) shows that certain self-attention blocks in Vision Transformers exhibit low feature entropy and can be merged into their subsequent MLPs without harming accuracy. In their approach, entropy is used as a post-hoc scoring metric: layers with lower entropy are identified as redundant and directly removed, but the method itself does not attempt to reduce entropy during training. By contrast, in our framework, unstructured pruning actively drives the entropy of neurons and layers downward, allowing them to naturally reach a linearizable state in which they can be safely removed. By prioritizing pruning connections in low-entropy layers, EGP (Liao et al., 2023) is also an unstructured entropy-guided pruning method that reduces DNN depth. Nevertheless, when EGP performs unstructured pruning, it classifies rectifier states into fewer categories than ours and does not account for the entropy of individual neurons.

Neural Network Depth Reduction. Towards neural network depth reduction, Structured Sparsity Learning (SSL) (Wen et al., 2016) uses group lasso regularization on the weights of each layer to determine which layers are less critical. This approach aims to reduce redundant layers with minor performance loss. However, SSL does not guarantee entire layer removal while maintaining model performance, as depth reduction is often achieved at the cost of accuracy degradation. Then, Chen & Zhao (2019) inspects the possibility of having a layer-wise pruning method based on feature representation, a-posteriori employing a retraining strategy that utilizes knowledge distillation. However, its effectiveness strongly depends on the retraining stage, and the additional knowledge distillation step increases training cost and limits scalability to larger models. Endorsing this, Dror et al. (2022) proposed a method that learns whether non-linear activations can be removed, allowing the folding of consecutive linear layers into one. More specifically, ReLU-activated layers are replaced with PReLU activations, showcasing a regularized slope. During post-training, the PReLUs almost linear are removed, and the layer can be folded with its subsequent one. Ali Mehmeti-Göpel & Disselhoff (2023) proposes a similar channel-wise approach that enables reducing more non-linear units in the network while maintaining similar performance. While previous methods attempted to reduce

network depth by constraining activations to remain either linear or non-linear, our approach reveals that unstructured pruning naturally leads the model to achieve this behavior without explicit enforcement. We demonstrate, both theoretically and empirically, that there exists the possibility of network layers "collapsing on their own" to reduce their depth, even with the classical unstructured pruning strategy. This finding provides a new perspective on network depth reduction.

3 Unstructured Pruning Induces Layer Collapse

In this section, we first introduce the notion of neuron entropy, which quantifies the degree of nonlinearity utilization (Sec. 3.1). Then, we show that unstructured pruning naturally minimizes the neuron’s entropy (in rectifier-activated layers) (Sec. 3.2). This motivates our entropy-guided pruning approach, which allows a gradual layer removal. Finally, we propose our method NEPENTHE, which focuses on pruning connections in layers with low entropy to remove them entirely (Sec. 3.3).

3.1 Entropy for Rectifier Activations

Let us assume ψ is the rectifier of the l -th layer, populated by N_l neurons. We can monitor the output $y_{l,i}^{\mathbf{x}}$ of the i -th neuron from a given input \mathbf{x} of the dataset \mathcal{D} and write it as:

$$y_{l,i}^{\mathbf{x}} = \psi(z_{l,i}^{\mathbf{x}}), \quad (1)$$

where $z_{l,i}^{\mathbf{x}}$ is the output of the i -th neuron inside the l -th layer. From equation 1, we can define three possible “states” for the neuron:

$$s_{l,i}^{\mathbf{x}} = \begin{cases} +1 & \text{if } z_{l,i}^{\mathbf{x}} > 0 \\ -1 & \text{if } z_{l,i}^{\mathbf{x}} < 0 \\ 0 & \text{if } z_{l,i}^{\mathbf{x}} = 0. \end{cases} \quad (2)$$

More synthetically, for the output of the i -th neuron, we can easily identify in which of these states we are by simply applying the sign function to $z_{l,i}^{\mathbf{x}}$, obtaining $s_{l,i}^{\mathbf{x}} = \text{sign}(z_{l,i}^{\mathbf{x}})$. Informally, we can say that the neuron is in the *ON State* when $s_{l,i}^{\mathbf{x}} = +1$ (as it is typically the linear region) while it is in the *OFF State* when $s_{l,i}^{\mathbf{x}} = -1$ (given that $\lim_{x \rightarrow -\infty} \psi(x) = 0$).¹ The third State $s_{l,i}^{\mathbf{x}} = 0$ is a special case, as it can be either mapped as an ON or OFF State. From the average over a batch of outputs for the neuron, we can obtain the probability (in the frequentist sense) of the i -th neuron of being in either the ON or the OFF States. For instance, we can obtain the probability of the ON State as:

$$p(s_{l,i} = +1) = \begin{cases} \frac{1}{S_{l,i}} \sum_{j=1}^{\|\mathcal{D}\|_0} s_{l,i}^{\mathbf{x}_j} \Theta(s_{l,i}^{\mathbf{x}_j}) & \text{if } S_{l,i} \neq 0 \\ 0 & \text{otherwise,} \end{cases} \quad (3)$$

where

$$S_{l,i} = \sum_{j=1}^{\|\mathcal{D}\|_0} |s_{l,i}^{\mathbf{x}_j}| \quad (4)$$

counts how many times the ON and the OFF states are encountered, $\|\mathcal{D}\|_0$ is the number of the input samples, and Θ is the Heaviside function.² Evidently, we exclude the third state from this count as it can be associated with being either within ON or OFF. Given that we are either interested in the ON or the OFF States, we can then deduce that, when $S_{l,i} \neq 0$, $p(s_{l,i} = -1) = 1 - p(s_{l,i} = +1)$. Given this, we can calculate the entropy of the i -th neuron in the l -th layer as follows:

$$\mathcal{H}_{l,i} = - \sum_{s_{l,i} = \pm 1} p(s_{l,i}) \log_2 [p(s_{l,i})]. \quad (5)$$

With the definition in equation 5, $\mathcal{H}_{l,i}$ can be zero in two possible cases:

¹There are few exceptions, such as LeakyReLU. In these cases, although the activation doesn’t converge to zero, we still call it the OFF state since the output’s magnitude is lower for the same input magnitude.

²For convolutional layers, it is necessary to sum and average over the entire feature map generated per input.

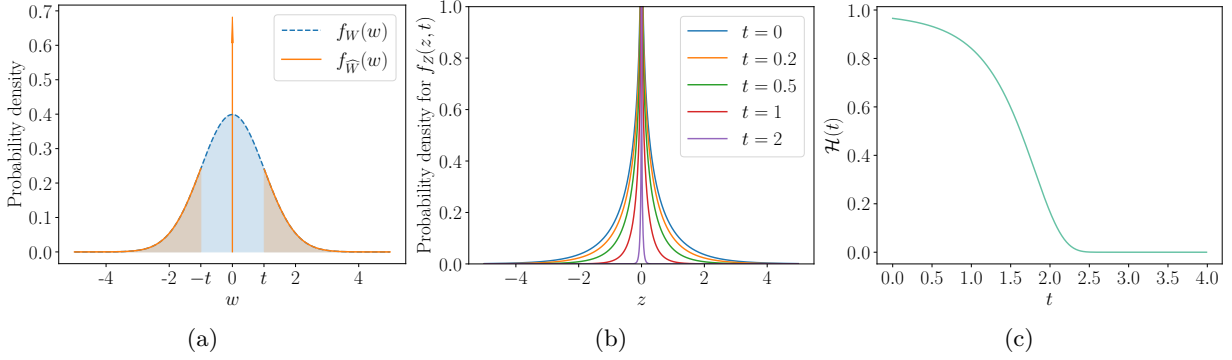


Figure 2: (a) Distribution of a layer’s parameters with magnitude pruning at threshold t ; (b) pre-activation distribution at varying t under the assumption of independence and centering of the Gaussian distributed input and layer’s parameters; (c) entropy of the rectifier-activated neuron’s output as a function of t , all in the large N limit.

- $s_{l,i} = -1 \forall j$. In this case, $z_{l,i} \leq 0 \forall j$. When employing a ReLU, the output of the i -th neuron is always 0, and in this specific case, the neuron can be simply pruned.
- $s_{l,i} = +1 \forall j$. In this case, $z_{l,i} \geq 0 \forall j$. When employing a ReLU, the output of the i -th neuron is always the same as its input, and the neuron can be absorbed by the following layer as there is no non-linearity between them anymore. For smooth rectifier variants such as GELU/SiLU, this process is an approximation where the error can be negligible. We formalize and bound this approximation error in Appendix A.

By averaging the entropy values for the total number of neurons N_l inside the l -th layer, we can define the average layer entropy of the l -th layer as:

$$\widehat{\mathcal{H}}_l = \frac{1}{N_l} \sum_i \mathcal{H}_{l,i}. \quad (6)$$

We refer to $\widehat{\mathcal{H}}_l$ as the average first-order layer entropy of layer l , i.e., the mean neural entropy across its neurons. This quantity is a scalable proxy for layer linearizability and is not intended to estimate the joint entropy of the layer’s activation-state vector.

Since we aim to minimize the depth of deep neural networks by eliminating zero-entropy layers, we would like to have $\widehat{\mathcal{H}}_l = 0$.

3.2 Unstructured Pruning Naturally Reduces the Entropy

Let us assume the input \mathbf{x} for a given neuron is a sequence of random variables $X \sim \mathcal{N}(\mu_X, \sigma_X^2)$. Similarly, we can assume the N parameters populating such neuron, for a large N limit, follow as well a Gaussian distribution, and we model it as $W \sim \mathcal{N}(\mu_W, \sigma_W^2)$. These assumptions are empirically validated in Appendix D.5. Let us assume we apply a magnitude-based pruning mask to the neuron’s parameters, where we apply some threshold t . As such, we obtain a modified distribution for the layer’s parameters:

$$f_{\widehat{W}}(w, t) = \begin{cases} \frac{1}{\sigma_W \sqrt{2\pi}} \exp \left[-\frac{1}{2} \left(\frac{w - \mu_W}{\sigma_W} \right)^2 \right] & |w| > t \\ \zeta(t) \delta(w) & |w| \leq t, \end{cases} \quad (7)$$

where

$$\zeta(t) = \frac{1}{2} \left[\operatorname{erf} \left(\frac{t - \mu_W}{\sigma_W \sqrt{2}} \right) - \operatorname{erf} \left(\frac{-t - \mu_W}{\sigma_W \sqrt{2}} \right) \right] \quad (8)$$

Algorithm 1 Our proposed method NEPENTHE.

```

1: function NEPENTHE( $\mathbf{w}^{\text{INIT}}, L, \mathcal{D}, \zeta, \theta$ )
2:    $\mathbf{w} \leftarrow \text{Train}(\mathbf{w}^{\text{init}}, \mathcal{D}_{\text{train}})$ 
3:    $\text{dense\_acc} \leftarrow \text{Evaluate}(\mathbf{w}, \mathcal{D}_{\text{val}})$ 
4:    $\text{current\_acc} \leftarrow \text{dense\_acc}$ 
5:   while  $\text{current\_acc} > \theta \cdot \text{dense\_acc}$  do
6:      $\hat{\mathcal{H}} \leftarrow \text{Entropy}(\mathbf{w}, L, \mathcal{D}_{\text{train}})$ 
7:      $\|\mathbf{w}\|_0^{\text{pruned}} \leftarrow \zeta \cdot \|\mathbf{w}\|_0$ 
8:      $\|\mathbf{w}_L\|_0^{\text{pruned}} \leftarrow \text{Weights\_to\_prune}(L, \hat{\mathcal{H}}, \|\mathbf{w}\|_0^{\text{pruned}}, \mathcal{D}_{\text{train}})$ 
9:      $\mathbf{w} \leftarrow \text{Prune}(\|\mathbf{w}_L\|_0^{\text{pruned}})$ 
10:     $\mathbf{w} \leftarrow \text{Train}(\mathbf{w}, \mathcal{D}_{\text{train}})$ 
11:     $\text{current\_acc} \leftarrow \text{Evaluate}(\mathbf{w}, \mathcal{D}_{\text{val}})$ 
12:  end while
13:  return  $\mathbf{w}$ 
14: end function

```

is the fraction of parameters pruned, or *pruning rate*, δ is the Dirac delta and erf is the error function. Fig. 2a displays an example of distribution when applying magnitude pruning having threshold t against the original distribution. Following Craig (1936), we work with the standardised variables

$$\tilde{X} = \frac{X - \mu_X}{\sigma_X}, \quad \tilde{W} = \frac{W - \mu_W}{\sigma_W},$$

so that $\tilde{X}, \tilde{W} \sim \mathcal{N}(0, 1)$, and with the normalised pre-activation

$$\tilde{Z} = \tilde{X}\tilde{W} = \frac{Z}{\sigma_X\sigma_W}.$$

For notational simplicity, we denote \tilde{Z} again by Z in what follows. Under the assumption of independent-centered distributions having a unitary variance, we can obtain the distribution for the pre-activation z (resulting from the product of the weights and the input, modeled through the random variable Z), according to the result obtained by Craig (1936); Seijas-Macías & Oliveira (2012), follows

$$f_Z(z, t) = \frac{1}{\pi} K_0 \left(\left| \frac{1}{q(t)} \cdot z \right| \right), \quad (9)$$

where

$$q(t) = 1 - \text{erf} \left(\frac{t}{\sqrt{2}} \right) \quad (10)$$

and K_n is the n -th order modified Bessel function of the second kind. We can observe, from Fig. 2b, how f_Z is affected by increasing the thresholding t . Now, let us assume the activation function of such a neuron is a rectifier function, and we are interested in observing what is the probability of the post-activation output being in the linear region: we are interested in measuring

$$p[Z > \varepsilon] = \frac{1}{\pi} \int_{\varepsilon}^{+\infty} K_0 \left(\left| \frac{1}{q(t)} \cdot z \right| \right) dz = \frac{1}{2} \left[1 - I \left(\frac{\varepsilon}{q(t)} \right) \right], \quad (11)$$

where

$$I(x) = x[L_{-1}(x)K_0(x) + L_0(x)K_1(x)], \quad (12)$$

L_n is the n -th order modified Struve function, and ε is a positive small value. From this, we can easily obtain the complementary probability $p[Z \leq \varepsilon]$ and for instance calculate the entropy between the two States.

Fig. 2c displays the entropy as a function of the thresholding parameter t : as we observe, the entropy decreases given that the threshold increases: through unstructured pruning, the neuron's output entropy is naturally minimized when employing rectified activations, even in the oversimplified case here treated.

In the following, we will present how we are exploiting such a property of unstructured pruning towards layer entropy minimization.

Algorithm 2 Function `Weights_to_prune`.

```

1: function WEIGHTS_TO_PRUNE( $L, \hat{\mathcal{H}}, \|\mathbf{w}\|_0^{\text{PRUNED}}, \mathcal{D}$ )
2:   for  $l \in L$  do
3:      $\mathcal{I}_l \leftarrow \frac{\|\mathbf{w}_l\|_1}{\|\mathbf{w}_l\|_0} \cdot \hat{\mathcal{H}}_l$ 
4:      $\mathcal{R}_l \leftarrow \begin{cases} \frac{\sum_{j \in L} \mathcal{I}_j}{\mathcal{I}_l} & \text{if } \mathcal{I}_l \neq 0 \\ 0 & \text{otherwise.} \end{cases}$ 
5:      $\|\mathbf{w}_l\|_0^{\text{pruned}} \leftarrow \|\mathbf{w}\|_0^{\text{pruned}} \cdot \frac{\exp[\mathcal{R}_l]}{\sum_j \exp[\mathcal{R}(j)]}$ 
6:   end for
7:   return  $\|\mathbf{w}_L\|_0^{\text{pruned}}$ 
8: end function

```

3.3 NEPENTHE

Driven by the promising theoretical results presented in Sec. 3.1 and Sec. 3.2, we design here NEPENTHE (eNtropy-basEd Pruning as a nEural Network depTH's rEducer) that guides the unstructured pruning to lower the whole layer's entropy $\hat{\mathcal{H}}_l$. Since we aim to increase the number of zero-entropy layers, intuitively more pruning should be applied to layers with lower entropy, as they are the best candidates to be removed. Concurrently, to minimize the impact on performance, only low-magnitude weights should be removed, as they are typically those providing the lowest contribution to the neural network's output (Han et al., 2015; Tartaglione et al., 2021). To reach these two objectives, we first define an intra-layer's pruning irrelevance score

$$\mathcal{I}_l = \frac{\|\mathbf{w}_l\|_1}{\|\mathbf{w}_l\|_0} \cdot \hat{\mathcal{H}}_l, \quad (13)$$

where $\|\mathbf{w}_l\|_0$ is the current layer's parameters cardinality (hence, not accounting for the already pruned weights, if any) and $\|\mathbf{w}_l\|_1$ is the ℓ_1 norm (sum of absolute values). This metric accounts for the average parameter's magnitude and the layer's entropy at the same time: layers with few parameters but high entropy are less prone to be removed than layers with more parameters but lower entropy (under the same parameter's norm constraint). Besides, the parameter's magnitude of neurons with zero entropy is not accounted for in the importance score calculation. Symmetrically, to remove parameters from layers having lower pruning irrelevance, we define the inter-layer's pruning relevance score \mathcal{R}_l as:

$$\mathcal{R}_l = \begin{cases} \frac{1}{\mathcal{I}_l} \sum_{j \in L} \mathcal{I}_j & \text{if } \mathcal{I}_l \neq 0 \\ 0 & \text{otherwise.} \end{cases} \quad (14)$$

This measure is as large as the l -th layer's pruning irrelevance score is smaller compared to the other layer's. Noticeably, $\mathcal{R}_l \in [1; +\infty)$: to exactly establish how many parameters $\|\mathbf{w}_l\|_0^{\text{pruned}}$ should be removed inside each layer l at a given pruning iteration, we have the *entropy-weighted pruned parameter budget*

$$\|\mathbf{w}_l\|_0^{\text{pruned}} = \|\mathbf{w}\|_0^{\text{pruned}} \cdot \frac{\exp[\mathcal{R}_l]}{\sum_j \exp[\mathcal{R}(j)]}. \quad (15)$$

In Alg. 1, we present a summary of NEPENTHE. Indeed, if a layer has an entropy equal to zero, then all of its neurons have an entropy equal to zero: $\hat{\mathcal{H}}_l = 0 \Leftrightarrow \mathcal{H}_{l,i} = 0, \forall i$. Hence, this layer doesn't necessarily need to have a rectifier: this layer can be removed entirely without the need for future pruning. Towards this end, we first train the neural network, represented by its weights at initialization \mathbf{w}^{init} , on the training set $\mathcal{D}_{\text{train}}$ (line 2) and evaluate it on the validation set \mathcal{D}_{val} (line 3). As defined in equation 6, we then calculate the entropy $\hat{\mathcal{H}}$ on the training set $\mathcal{D}_{\text{train}}$ for each layer l of the considered list of layers L (line 6). This list is initialized to all the layers of the neural network having a rectifier activation (hence, the output layer is excluded).

Considering that ζ represents the percentage of parameters to remove at each pruning iteration and $\|\mathbf{w}\|_0$ the total weight parameters of the considered L layers in the model, we can define the number of weight

parameters to be pruned at each iteration $\|\mathbf{w}\|_0^{\text{pruned}}$ (line 7) as:

$$\|\mathbf{w}\|_0^{\text{pruned}} = \zeta \cdot \|\mathbf{w}\|_0. \quad (16)$$

To determine the parameters to prune in each layer, we define a function `Weights_to_prune`, as presented in Alg. 2. This function calculates the weights to remove for each layer and returns a list indicating the number of neurons that need to be removed from each layer, as discussed in Sec. 3.3. At this point, for each layer l , the neurons having non-zero entropy are first selected and then $\|\mathbf{w}_l\|_0^{\text{pruned}}$ non-zero weights having the lowest absolute magnitude are removed (line 9). The model is then retrained (line 10) and re-evaluated on the validation set \mathcal{D}_{val} (line 11). The final model is obtained once the performance on the validation set drops below some relative threshold θ .

4 Experiments

In this section, we empirically apply unstructured magnitude pruning across multiple architectures and datasets for traditional image classification and natural language processing setups to validate the mechanism: whether unstructured pruning can lower layer entropy and yield zero-entropy, linearizable layers with no performance degradation. We further analyze how pruning affects each layer’s entropy and the model’s loss landscape sharpness.

Then, we compare NEPENTHE with the iterative magnitude pruning (IMP) baseline from Han et al. (2015). Additionally, in image classification tasks, we compare our results with two other approaches: removing the layers having the lowest sum of weights/gradients. These baselines serve as naive structural criteria that directly measure layer importance without considering activation behavior, allowing us to isolate the specific contribution of entropy-based guidance. We further induce intra-layer sparsity using HRank (Lin et al., 2020), a filter pruning method that removes filters with low-rank feature maps. This comparison highlights the distinction between width-oriented compression and our depth-reduction strategy. In addition, we minimize the group lasso penalty for each layer following the approach of Ochiai et al. (2017). We also compare our method with EGP (Liao et al., 2023), which removes layers through an unstructured pruning process and represents the work most closely related to ours. Furthermore, we demonstrate that our approach can be combined with structured pruning, suggesting promising directions for future pruning method development.

4.1 Experimental setup

A variety of setups is covered by evaluating our method on three popular image classification models: ResNet-18 (He et al., 2016), MobileNet-V2 (Howard et al., 2017), and Swin-T (Liu et al., 2021), trained on five datasets: CIFAR-10 (Krizhevsky et al., 2009), Tiny-ImageNet (Le & Yang, 2015), and PACS, VLCS, and SVIRO from DomainBed (Gulrajani & Lopez-Paz, 2021), following the same training policies as Quéto & Tartaglione (2024) and Xu et al. (2021). Moreover, two natural language processing models: BERT (Kenton & Toutanova, 2019) and RoBERTa (Liu et al., 2019) are trained on three datasets: SST-2 (Socher et al., 2013), QNLI (Williams et al., 2018), and RTE (Bentivogli et al., 2009), following the training strategies of Peer et al. (2022). To verify the generality of the layer collapse phenomenon induced by unstructured pruning across models with different depths and widths, as well as on datasets of higher complexity, NEPENTHE has also been implemented for ResNet-50, ResNet-152, and MobileNetV2-0.75 models trained on CIFAR-10, as well as ResNet-18 trained on ImageNet (Deng et al., 2009). Results appear in Appendix D.2. In all the setups, we set $\zeta = 0.5$ for ResNet-18,

Table 1: Trend in the bottom six layers’ entropies for ResNet-18 trained on CIFAR-10.

Approach	$\hat{\mathcal{H}}_1$	$\hat{\mathcal{H}}_2$	$\hat{\mathcal{H}}_3$	$\hat{\mathcal{H}}_4$	$\hat{\mathcal{H}}_5$	$\hat{\mathcal{H}}_6$	top-1
Dense	0.647	0.680	0.728	0.785	0.791	0.797	91.66
IMP (iter #1)	0.585	0.650	0.699	0.725	0.767	0.778	92.29
IMP (iter #2)	0.506	0.580	0.647	0.654	0.700	0.722	92.25
IMP (iter #3)	0.256	0.623	0.658	0.672	0.682	0.737	92.46
IMP (iter #4)	0.192	0.660	0.667	0.676	0.698	0.763	92.27
IMP (iter #5)	0.136	0.589	0.648	0.727	0.728	0.791	92.44
IMP (iter #6)	0.093	0.447	0.640	0.650	0.764	0.765	91.89
IMP (iter #7)	0.055	0.335	0.487	0.592	0.640	0.775	91.66
NEPENTHE	0	0	0	0.014	0.121	0.942	92.55

Table 2: Test performance (top-1) and the number of removed layers (Rem.) for all the considered image classification setups. The results achieved by our method are in italics.

Model	Approach	CIFAR-10		Tiny-ImageNet		PACS		VLCS		SVIRO	
		top-1	Rem.	top-1	Rem.	top-1	Rem.	top-1	Rem.	top-1	Rem.
ResNet-18	Dense	91.66	0/17	41.44	0/17	94.70	0/17	80.89	0/17	99.93	0/17
	Smallest weights	10.00	1/17	0.5	1/17	16.20	1/17	46.13	1/17	35.55	1/17
	Smallest gradients	9.29	1/17	0.5	1/17	16.20	1/17	46.13	1/17	35.55	1/17
	Hrank	91.70	0/17	-	-	-	-	-	-	-	-
	Group lasso	92.11	1/17	38.92	0/17	81.20	0/17	67.85	0/17	99.57	0/17
	IMP	91.66	0/17	39.14	0/17	89.80	0/17	74.09	0/17	99.45	0/17
	EGP	92.18	3/17	39.50	4/17	84.30	2/17	74.28	2/17	98.66	5/17
	<i>NEPENTHE</i>	92.55	3/17	39.56	5/17	90.10	3/17	78.38	2/17	99.61	8/17
MobileNet-V2	Dense	93.68	0/35	45.86	0/35	93.20	0/35	81.83	0/35	99.95	0/35
	Smallest weights	10.00	1/35	0.50	1/35	18.50	1/35	6.43	1/35	35.55	1/35
	Smallest gradients	10.00	1/35	46.62	1/35	16.20	1/35	46.13	1/35	35.55	1/35
	Hrank	91.73	0/35	-	-	-	-	-	-	-	-
	Group lasso	83.00	4/35	47.1	0/35	92.10	0/35	78.84	0/35	99.93	0/35
	IMP	92.50	0/35	45.24	0/35	91.40	0/35	79.43	0/35	99.95	0/35
	EGP	92.22	6/35	47.52	6/35	17.70	3/35	45.85	2/35	35.05	2/35
	<i>NEPENTHE</i>	93.26	7/35	47.92	12/35	92.20	<i>1/35</i>	80.06	2/35	99.98	2/35
Swin-T	Dense	91.54	0/12	75.60	0/12	97.10	0/12	86.58	0/12	99.95	0/12
	Smallest weights	89.22	2/12	75.12	1/12	96.10	2/12	84.62	1/12	99.70	4/12
	Smallest gradients	89.21	2/12	74.54	1/12	95.70	2/12	84.15	1/12	99.55	4/12
	Hrank	91.87	0/12	-	-	-	-	-	-	-	-
	Group lasso	91.68	0/12	71.30	0/12	94.30	0/12	84.81	0/12	99.69	0/12
	IMP	90.53	0/12	67.56	0/12	93.90	0/12	80.06	0/12	99.75	0/12
	EGP	92.01	1/12	71.48	1/12	93.50	1/12	82.95	1/12	99.64	5/12
	<i>NEPENTHE</i>	92.29	2/12	<i>72.58</i>	1/12	<i>95.10</i>	2/12	85.27	1/12	99.75	5/12

Table 3: Trend for the model’s Sharpness for Swin-T trained on CIFAR-10.

Approach	Sharpness	top-1	Rem.
Dense	20.62	91.54	0/12
IMP (iter #1)	6.78	91.73	0/12
IMP (iter #2)	3.70	91.80	0/12
IMP (iter #3)	3.18	91.43	0/12
IMP (iter #4)	4.78	91.46	0/12
IMP (iter #5)	5.39	91.27	0/12
IMP (iter #6)	6.81	91.05	0/12
IMP (iter #7)	7.66	90.53	0/12
<i>NEPENTHE</i> (iter #1)	7.71	91.77	0/12
<i>NEPENTHE</i> (iter #2)	2.82	92.06	0/12
<i>NEPENTHE</i> (iter #3)	1.58	92.08	0/12
<i>NEPENTHE</i> (iter #4)	1.17	92.31	0/12
<i>NEPENTHE</i> (iter #5)	1.85	92.29	2/12
<i>NEPENTHE</i> (iter #6)	1.62	92.21	2/12
<i>NEPENTHE</i> (iter #7)	1.72	92.11	2/12

Table 4: Test performance (top-1) and the number of removed layers (Rem.) for all the considered NLP setups. The results achieved by our method are in italics.

Dataset	Approach	BERT		RoBERTa	
		top-1	Rem.	top-1	Rem.
QNLI	Dense	90.48	0/12	92.18	0/12
	Smallest weights	88.15	3/12	85.93	2/12
	Smallest gradients	88.44	3/12	86.84	2/12
	IMP	85.87	0/12	88.10	0/12
	EGP	87.90	4/12	84.66	2/12
	<i>NEPENTHE</i>	88.69	4/12	<i>87.41</i>	2/12
RTE	Dense	61.01	0/12	66.79	0/12
	Smallest weights	46.93	1/12	65.81	1/12
	Smallest gradients	55.23	1/12	62.20	1/12
	IMP	57.76	0/12	62.82	0/12
	EGP	57.73	1/12	52.71	1/12
	<i>NEPENTHE</i>	58.12	4/12	66.06	1/12
SST-2	Dense	92.20	0/12	92.66	0/12
	Smallest weights	88.14	3/12	89.43	4/12
	Smallest gradients	87.25	3/12	89.43	4/12
	IMP	88.65	0/12	88.76	0/12
	EGP	85.09	3/12	86.47	4/12
	<i>NEPENTHE</i>	88.99	3/12	89.79	4/12

$\zeta = 0.25$ for Swin-T, and $\zeta = 0.1$ for MobileNet-V2. Moreover, we set $\zeta = 0.25$ (respectively $\zeta = 0.15$) for the models trained on QNLI and RTE (respectively SST-2). All the hyperparameters, augmentation strategies, learning policies, and a study to choose ζ are provided in Appendix C.

4.2 Trend of Layer’s Entropy and Model’s Sharpness

First, we study the effect of pruning on the layer’s entropy. Table 1 reports the entropy trend of the six layers having the lowest entropy for ResNet-18 trained on CIFAR-10. As expected from the derivation in Sec. 3.1, as the pruning progresses (and implicitly as t grows), the entropy is naturally decreased, showcasing very small values after some pruning iterations. However, we also observe that as the entropy \hat{H}_1 decreases, the top-1 accuracy begins to deteriorate. This occurs without proper pruning reallocation, unlike in NEPENTHE with equation 14. Indeed, in this case, our method not only preserves the model performance (even improves it),

but we can also successfully remove three layers from the model. Noticeably, \hat{H}_4 and \hat{H}_5 are also very low, while already starting from \hat{H}_6 , the entropy is very high. As opposed to IMP where in general the entropy lies in intermediate-range values, NEPENTHE tries to push all the encoded information toward layers having already high entropy, enabling effective layer removal with little (or in this case no) performance loss. This is also illustrated in Fig. 3, showing the distribution of the filter states per layer for the same setup. Our unstructured pruning approach effectively removes three layers by pushing all the neurons inside low-entropy layers to be either in the ON or in the OFF state. Besides, we also notice that in some layers (like 13 and 17), entire units reach zero entropy, indicating that structured sparsity can naturally emerge from an unstructured pruning process, as previously reported in related works (Han et al., 2015; Tartaglione et al., 2021).

Moreover, we analyze the layers pruned from a ResNet-18 trained on CIFAR-10 by other baselines in Appendix D.1. While with NEPENTHE, the layers with the lowest entropy are typically found near the deepest layers of the network, the layers near the output are often pruned first with EGP (Fig. 6c). This happens because the layers near the output usually capture highly task-specific or redundant features whose removal causes limited disturbance to earlier representations, allowing the network to retain most of its predictive capacity. In contrast, methods that prune layers based on the lowest sum of weights/gradients tend to remove layers near the input of the model first (Fig. 6a and Fig. 6b). These early layers have fewer parameters and smaller cumulative sums, making them appear less important. Once removed, however, the forward signal is broken and the model’s accuracy drops to a random level.

Table 3 shows how pruning affects loss landscape sharpness for Swin-T on CIFAR-10 trained with IMP and NEPENTHE. Following Lee et al. (2025), we compute the maximum Hessian eigenvalues to measure the sharpness of the models. Lower sharpness values correspond to flatter loss surfaces. As in previous studies (Liebenwein et al., 2021), IMP is able to reduce the model’s loss landscape sharpness at moderate or low sparsity, but the sharpness increases at higher sparsity. Unlike IMP, NEPENTHE can significantly reduce the model’s loss landscape and improve generalization.

4.3 Main Results

Image classification tasks. Table 2 shows the test performance (top-1) and the number of removed layers (Rem.) for all the considered image classification setups. Removing layers with the lowest weight/gradient sums only works for Swin-T. On ResNet-18 and MobileNet-V2, these methods reduce accuracy to random levels after one layer removal. Since Hrank operates at the level of the neuron, even though it can help models maintain a good (or even better) performance after pruning, no layer can be removed with this method. Thus, we report Hrank results only for CIFAR-10 to save computational resources. Moreover, although minimizing the group lasso penalty has little impact on the performance, its effectiveness in layer removal is not significant. Furthermore, IMP does not support the removal of any layers despite successfully maintaining performance. However, EGP enables the removal of some layers but at the expense of compromising generalizability. For example, on MobileNet-V2 trained on PACS, EGP removes three layers outright, leading to a significant drop in accuracy. In contrast, NEPENTHE produces models with a substantial number of removable layers with little (or no) performance loss compared to the dense baseline. For instance, on

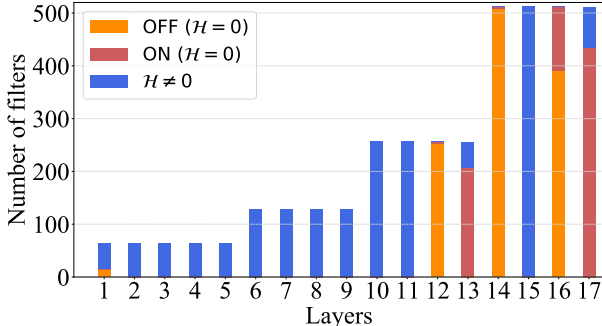


Figure 3: Filter states per layer for ResNet-18 trained on CIFAR-10 pruned by NEPENTHE.

Table 5: Ablation study on ResNet-18 trained on CIFAR-10. Each component contributes to the effectiveness of NEPENTHE.

Entropy-based budget	Don't care state	Neurons selection	top-1	Rem.
			91.66	0/17
✓			92.18	3/17
✓	✓		92.33	3/17
✓	✓	✓	92.55	3/17
Depth reduced model trained from initialization			91.57	3/17

Table 6: MobileNet-V2 with ReLU6 trained on CIFAR-10 dataset.

Method	top-1	Rem.
Dense	93.68	0/35
NEPENTHE	93.55	1/35
NEPENTHE	93.25	2/35
NEPENTHE	93.37	4/35
NEPENTHE	93.15	5/35
NEPENTHE	93.26	7/35
NEPENTHE	92.78	9/35

MobileNet-V2 trained on Tiny-ImageNet, NEPENTHE successfully removes 12 layers while even improving the top-1 accuracy by about 2%.

NLP tasks. The results for all NLP setups are presented in Table 4. Similarly to what was observed for image classification setups, we observe that while IMP does not significantly harm performance, it does not support whole-layer removal. In contrast, NEPENTHE produces models with a significant number of removable layers while maintaining a performance comparable to the dense models.

4.4 Combination of Unstructured Pruning and Structured Pruning Methods

Besides pure unstructured pruning, we also explore the potential of combining NEPENTHE with structured layer removal methods to extend its applicability. In particular, we integrate the group lasso regularization used in SSL with NEPENTHE. Fig. 4 shows the results of this combination. Although a slight drop in accuracy is observed when fewer layers are pruned compared with pure NEPENTHE, the joint approach enables the removal of a larger number of layers while maintaining competitive performance. This demonstrates NEPENTHE’s flexibility and its potential to serve as a general framework that can be coupled with various structured sparsity or layer-selection techniques to achieve both entropy-driven and structure-aware depth reduction.

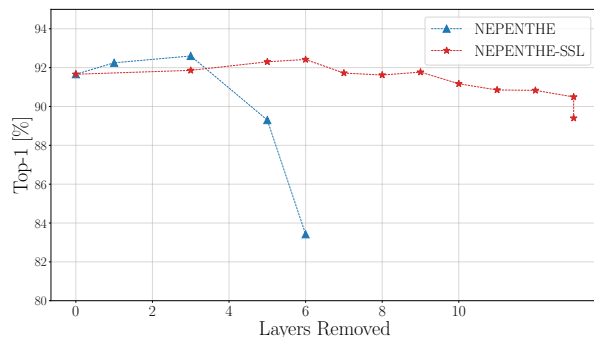


Figure 4: Test performance (top-1) and the number of removed layers (Rem.) for ResNet-18 trained on CIFAR-10.

4.5 Ablation Study

In this section, we conduct several studies. First, we perform a classical ablation to analyze the contribution of each term within NEPENTHE. Second, we verify the layer collapse phenomenon induced by unstructured pruning using some of the most common two-interval rectifiers. Then, we extend this validation to rectifiers with more intervals. Moreover, we test the phenomenon beyond magnitude-based pruning by applying it to Wanda. Finally, we demonstrate the practical benefits of our approach in terms of inference time, memory usage, and energy consumption.

First, Table 5 provides an ablation study on the three key components identifiable within NEPENTHE: the entropy-based weighted pruned parameter budget (equation 13), the presence of the don’t care state in the entropy formulation (equation 2), and the filtering mechanism of non-zero entropy neurons (equation 13). In table 5, we also report a depth-matched baseline trained from initialization. The results show that each component contributes to the overall effectiveness of NEPENTHE, jointly enhancing both pruning stability and the emergence of layer collapse.

Table 7: Test performance (top-1) and the number of removed layers (Rem.) for ResNet-18 trained on CIFAR-10 dataset and pruned by combining NEPENTHE and Wanda.

Method	top-1	Rem.
Dense	91.66	0/17
NEPENTHE Wanda	92.67	1/17
NEPENTHE Wanda	89.80	3/17
NEPENTHE Wanda	89.37	5/17
NEPENTHE Wanda	88.31	6/17

Table 8: The accuracy and number of layers removable for Llama 3.1-8B (16FP) evaluated on MMLU - High school US history and pruned by NEPENTHE without fine-tuning (no ft).

Method	Val top-1	Test top-1	Rem.
Dense	40.91	33.82	0/32
NEPENTHE (no ft)	38.49	36.76	3/32
NEPENTHE (no ft)	36.36	29.90	5/32
NEPENTHE (no ft)	33.82	35.08	7/32
NEPENTHE (no ft)	31.82	28.92	9/32
NEPENTHE (no ft)	18.18	27.45	11/32

Second, Table 9 shows the test performance of ResNet-18 on CIFAR-10 and pruned by NEPENTHE, for different rectifiers. The fact that unstructured pruning induces layer collapse is not dependent on any particular rectifier and can be effective with any, since our method removes three layers without performance loss for all the tested activations.

Moreover, we evaluate NEPENTHE on MobileNet-V2 with ReLU6 trained on CIFAR-10. Table 6 shows the results, indicating that NEPENTHE can remove layers with minimal performance loss. Note that ReLU6 is a rectifier divided into three intervals, suggesting that this layer collapse phenomenon also appears in models with rectifiers that have more states. We present the theory analysis for rectifiers with more than two intervals in Appendix B.

Furthermore, Table 7 presents the results of applying Wanda pruning within the NEPENTHE framework for ResNet-18 on CIFAR-10. In this setting, we replace magnitude pruning with Wanda as the underlying pruning criterion. With one layer removed, the model even achieves better performance, confirming that the layer collapse phenomenon induced by unstructured pruning is not limited to magnitude-based strategies but also arises under other popular methods such as Wanda.

Finally, Table 10 showcases the potential savings in terms of inference time, memory usage, and energy consumption on an NVIDIA A4500 GPU for a ResNet-18 trained on CIFAR-10 with NEPENTHE: the fewer layers the network has, the lower the inference time, the smaller the memory usage and energy consumption. Note that FLOPs do not necessarily decrease due to the fact that composing consecutive linear operators may not preserve unstructured sparsity; we clarify this point in Appendix D.3.

4.6 Limitations

The work here presented shows two major limitations that will be tackled in future work.

The first limitation is related to the established theoretical framework. While our main objective is to shed light over the mechanism by which unstructured pruning drives rectifier-activated layers toward a low-entropy regime, the analysis is limited to ReLU activations. We derive in the supplementary material error bounds for other popular rectifiers; nevertheless this results in a limitation of the conducted analysis. Moreover, since $\hat{\mathcal{H}}_l$ averages first-order neuron entropies, that represents nothing but a proxy for linearizability rather than the joint entropy of the layer’s activation-state pattern.

Table 9: Different activation functions on ResNet-18 trained on CIFAR-10.

Activation	Method	top-1	Rem.
ReLU	Dense	91.66	0/17
	NEPENTHE	92.55	3/17
SiLU	Dense	91.66	0/17
	NEPENTHE	92.77	3/17
PReLU	Dense	91.25	0/17
	NEPENTHE	92.27	3/17
LeakyReLU	Dense	91.66	0/17
	NEPENTHE	92.49	3/17
GELU	Dense	91.89	0/17
	NEPENTHE	92.57	3/17

Table 10: Inference time [ms], Memory usage [MBs] and Energy consumption [mJ] of ResNet-18 on CIFAR-10 on a NVIDIA A4500.

Rem.	Inference time [ms]	Mem.usage [MBs]	Energy [mJ]	top-1
0/17	3.32	230	498.7	91.66
1/17	3.27	202	490.2	92.25
3/17	2.96	170	444.0	92.55
5/17	2.60	60	389.7	89.30

The second limitation involves the iterative nature of NEPENTHE can limit its direct application to very large models, as repeated pruning and retraining cycles are computationally demanding. To keep the study tractable, our main experiments focus on moderate-scale architectures, with the corresponding training time analysis provided in Appendix D.4. Nevertheless, to illustrate the broader applicability of our approach, we apply NEPENTHE to a pre-trained Llama 3.1-8B model without any fine-tuning. As shown in Table 8, the method still performs reliably, indicating that it can scale to larger language models and remain effective in more complex scenarios. Future work will explore strategies to reduce iteration cost and further improve scalability.

5 Conclusion

In this work, we show that unstructured pruning can inherently induce structural effects in deep neural networks. Specifically, in rectifier-activated architectures, it naturally reduces neuron entropy, and when a layer’s average entropy reaches zero, that layer becomes linearizable and can be safely removed without degrading representational capacity. Building on this observation, we introduced NEPENTHE, an entropy-guided unstructured pruning framework that reallocates pruning budgets toward low-entropy layers. This enables networks to collapse redundant layers while preserving or even improving accuracy. Across diverse architectures and datasets, NEPENTHE removes layers with minimal or no performance loss and yields flatter landscapes, better generalization, and efficiency gains.

Beyond empirical results, this study provides a new theoretical perspective: unstructured pruning can serve as an implicit depth-regularization mechanism, driving networks toward simpler and more linear representations. We hope that this study encourages further investigation into how apparently “unstructured” operations can yield structural behaviors in deep networks.

Acknowledgments

This work received support from the European Union’s HORIZON Research and Innovation Programme under grant agreement No. 101120657, as part of the ENFIELD project (European Lighthouse to Manifest Trustworthy and Green AI). Additionally, funding was provided by the French National Research Agency (ANR) under grant agreements ANR-22-PEFT-0003 and ANR-22-PEFT-0007, as part of the France 2030 initiative, specifically the NF-NAI and NF-FITNESS projects. This work was also supported by the French National Research Agency (ANR) in the framework of the IA Cluster project “Hi! PARIS Cluster 2030” under Grant ANR-23-IACL-005, and by the Hi! PARIS Center on Data Analytics and Artificial Intelligence. Zhu Liao acknowledges financial support from the China Scholarship Council(CSC).

References

- Christian H.X. Ali Mehmeti-Göpel and Jan Disselhoff. Nonlinear advantage: Trained networks might not be as complex as you think. In *ICML*, 2023.
- Berker Arslan, Sefer Memiş, Elena Battini Sönmez, and Okan Zafer Batur. Fine-grained food classification methods on the uec food-100 database. *IEEE Transactions on Artificial Intelligence*, 2022.
- Luisa Bentivogli, Peter Clark, Ido Dagan, and Danilo Giampiccolo. The fifth pascal recognizing textual entailment challenge. *TAC*, 2009.
- Davis Blalock, Jose Javier Gonzalez Ortiz, Jonathan Frankle, and John Guttag. What is the state of neural network pruning? *MLSys*, 2020.
- Andrea Bragagnolo, Enzo Tartaglione, Attilio Fiandrotti, and Marco Grangetto. On the role of structured pruning for neural network compression. In *ICIP*, 2021.
- Shi Chen and Qi Zhao. Shallowing deep networks: Layer-wise pruning based on feature representations. *IEEE Transactions on Pattern Analysis and Machine Intelligence*, 2019.
- Cecil C Craig. On the frequency function of xy . *The Annals of Mathematical Statistics*, 1936.
- Jia Deng, Wei Dong, Richard Socher, Li-Jia Li, Kai Li, and Li Fei-Fei. Imagenet: A large-scale hierarchical image database. In *CVPR*, 2009.
- Amir Ben Dror, Niv Zehngut, Avraham Raviv, Evgeny Artyomov, Ran Vitek, and Roy Jevnisek. Layer folding: Neural network depth reduction using activation linearization. *BMVC*, 2022.
- Trevor Gale, Erich Elsen, and Sara Hooker. The state of sparsity in deep neural networks. *arXiv preprint arXiv:1902.09574*, 2019.
- Ishaan Gulrajani and David Lopez-Paz. In search of lost domain generalization. In *ICLR*, 2021.
- Jianyuan Guo, Kai Han, Han Wu, Yehui Tang, Xinghao Chen, Yunhe Wang, and Chang Xu. Cmt: Convolutional neural networks meet vision transformers. In *CVPR*, 2022.
- Song Han, Jeff Pool, John Tran, and William Dally. Learning both weights and connections for efficient neural network. *NeurIPS*, 2015.
- Kaiming He, Xiangyu Zhang, Shaoqing Ren, and Jian Sun. Deep residual learning for image recognition. In *CVPR*, 2016.
- Yang He and Lingao Xiao. Structured pruning for deep convolutional neural networks: A survey. *IEEE Transactions on Pattern Analysis and Machine Intelligence*, 2023.
- Zheng He, Zeke Xie, Quanzhi Zhu, and Zengchang Qin. Sparse double descent: Where network pruning aggravates overfitting. In *ICML*, 2022.
- Joel Hestness, Sharan Narang, Newsha Ardalani, Gregory Diamos, Heewoo Jun, Hassan Kianinejad, Md Mostofa Ali Patwary, Yang Yang, and Yanqi Zhou. Deep learning scaling is predictable, empirically. *arXiv preprint arXiv:1712.00409*, 2017.
- Andrew G Howard, Menglong Zhu, Bo Chen, Dmitry Kalenichenko, Weijun Wang, Tobias Weyand, Marco Andreetto, and Hartwig Adam. Mobilenets: Efficient convolutional neural networks for mobile vision applications. *arXiv preprint arXiv:1704.04861*, 2017.
- Cheonghwan Hur and Sanggil Kang. Entropy-based pruning method for convolutional neural networks. *The Journal of Supercomputing*, 2019.
- Jacob Devlin Ming-Wei Chang Kenton and Lee Kristina Toutanova. Bert: Pre-training of deep bidirectional transformers for language understanding. In *NAACL-HLT*, 2019.

- Alex Krizhevsky, Geoffrey Hinton, et al. Learning multiple layers of features from tiny images, 2009.
- Ya Le and Xuan Yang. Tiny imagenet visual recognition challenge. *CS 231N*, 2015.
- Dongyeop Lee, Kwanhee Lee, Jinseok Chung, and Namhoon Lee. Safe: Finding sparse and flat minima to improve pruning. *ICML*, 2025.
- Namhoon Lee, Thalaiyasingam Ajanthan, and Philip Torr. Snip: Single-shot network pruning based on connection sensitivity. In *ICLR*, 2019.
- Zhu Liao, Victor Quétu, Van-Tam Nguyen, and Enzo Tartaglione. Can unstructured pruning reduce the depth in deep neural networks? In *ICCV*, 2023.
- Lucas Liebenwein, Ramin Hasani, Alexander Amini, and Daniela Rus. Sparse flows: Pruning continuous-depth models. *NeurIPS*, 2021.
- Mingbao Lin, Rongrong Ji, Yan Wang, Yichen Zhang, Baochang Zhang, Yonghong Tian, and Ling Shao. Hrank: Filter pruning using high-rank feature map. In *CVPR*, 2020.
- Sihao Lin, Pumeng Lyu, Dongrui Liu, Tao Tang, Xiaodan Liang, Andy Song, and Xiaojun Chang. Mlp can be a good transformer learner. In *CVPR*, 2024.
- Yinhan Liu, Myle Ott, Naman Goyal, Jingfei Du, Mandar Joshi, Danqi Chen, Omer Levy, Mike Lewis, Luke Zettlemoyer, and Veselin Stoyanov. Roberta: A robustly optimized bert pretraining approach. *arXiv preprint arXiv:1907.11692*, 2019.
- Ze Liu, Yutong Lin, Yue Cao, Han Hu, Yixuan Wei, Zheng Zhang, Stephen Lin, and Baining Guo. Swin transformer: Hierarchical vision transformer using shifted windows. In *ICCV*, 2021.
- Christos Louizos, Max Welling, and Diederik P. Kingma. Learning sparse neural networks through l_0 regularization. In *ICLR*, 2018.
- Zhichao Lu, Ran Cheng, Shihua Huang, Haoming Zhang, Changxiao Qiu, and Fan Yang. Surrogate-assisted multiobjective neural architecture search for real-time semantic segmentation. *IEEE Transactions on Artificial Intelligence*, 2022.
- Jian-Hao Luo and Jianxin Wu. An entropy-based pruning method for cnn compression. *arXiv preprint arXiv:1706.05791*, 2017.
- Chuhan Min, Aosen Wang, Yiran Chen, Wenyao Xu, and Xin Chen. 2pfpc: Two-phase filter pruning based on conditional entropy. *arXiv preprint arXiv:1809.02220*, 2018.
- Tsubasa Ochiai, Shigeki Matsuda, Hideyuki Watanabe, and Shigeru Katagiri. Automatic node selection for deep neural networks using group lasso regularization. In *ICASSP*, 2017.
- David Peer, Sebastian Stabinger, Stefan Engl, and Antonio Rodríguez-Sánchez. Greedy-layer pruning: Speeding up transformer models for natural language processing. *Pattern Recognition Letters*, 2022.
- Victor Quétu and Enzo Tartaglione. Dsd²: Can we dodge sparse double descent and compress the neural network worry-free? In *AAAI*, 2024.
- Victor Quétu, Zhu Liao, and Enzo Tartaglione. The simpler the better: An entropy-based importance metric to reduce neural networks’ depth. In *ECML-PKDD*, 2024.
- Antonio Seijas-Macías and Amílcar Oliveira. An approach to distribution of the product of two normal variables. *Discussiones Mathematicae Probability and Statistics*, 2012.
- Richard Socher, Alex Perelygin, Jean Wu, Jason Chuang, Christopher D Manning, Andrew Y Ng, and Christopher Potts. Recursive deep models for semantic compositionality over a sentiment treebank. In *EMNLP*, 2013.

- Dongdong Sun, Minghui Wang, and Ao Li. A multimodal deep neural network for human breast cancer prognosis prediction by integrating multi-dimensional data. *IEEE/ACM Transactions on Computational Biology and Bioinformatics*, 2018.
- Mingjie Sun, Zhuang Liu, Anna Bair, and J. Zico Kolter. A simple and effective pruning approach for large language models. *ICLR*, 2024.
- Enzo Tartaglione, Andrea Bragagnolo, Francesco Odierna, Attilio Fiandrotti, and Marco Grangetto. Serene: Sensitivity-based regularization of neurons for structured sparsity in neural networks. *IEEE Transactions on Neural Networks and Learning Systems*, 2021.
- Enzo Tartaglione, Andrea Bragagnolo, Attilio Fiandrotti, and Marco Grangetto. Loss-based sensitivity regularization: towards deep sparse neural networks. *Neural Networks*, 2022.
- Hugo Touvron, Thibaut Lavril, Gautier Izacard, Xavier Martinet, Marie-Anne Lachaux, Timothée Lacroix, Baptiste Rozière, Naman Goyal, Eric Hambro, Faisal Azhar, et al. Llama: Open and efficient foundation language models. *arXiv preprint arXiv:2302.13971*, 2023.
- Wei Wen, Chunpeng Wu, Yandan Wang, Yiran Chen, and Hai Li. Learning structured sparsity in deep neural networks. *NeurIPS*, 2016.
- Adina Williams, Nikita Nangia, and Samuel R Bowman. A broad-coverage challenge corpus for sentence understanding through inference. In *NAACL*, 2018.
- Qinwei Xu, Ruipeng Zhang, Ya Zhang, Yanfeng Wang, and Qi Tian. A fourier-based framework for domain generalization. In *CVPR*, 2021.
- Chunjie Zhang, Ping Cao, Huihui Bai, and Xiaolong Zheng. Semantic coherence guided multiview similarity for image classification with varied supervision. *IEEE Transactions on Artificial Intelligence*, 2023.
- Michael H Zhu and Suyog Gupta. To prune, or not to prune: exploring the efficacy of pruning for model compression. *arXiv preprint arXiv:1710.01878*, 2017.

A Approximation Error for Smooth Rectifiers

For smooth rectifiers (e.g., GELU/SiLU), $\psi(z)$ is not exactly the identity even when $z > 0$, and that collapsing such layers is not a mathematically lossless operation. In this section, we formalize the approximation error and show why this error is negligible under the training and pruning regime considered in this work.

Consider a neuron with pre-activation

$$z(x) = w^\top x + b, \quad (17)$$

and a smooth rectifier activation $\phi \in \{\text{GELU}, \text{SiLU}\}$. Removing the activation corresponds to replacing $\phi(z)$ by the identity map z . The induced neuron-level approximation error is

$$\varepsilon(x) := \phi(z(x)) - z(x). \quad (18)$$

Since layer removal is evaluated at the dataset level, the relevant quantity is the expected squared error

$$\mathcal{E} := \mathbb{E}_{x \sim \mathcal{D}} [\|\phi(z(x)) - z(x)\|^2]. \quad (19)$$

Both GELU and SiLU admit the decomposition

$$\phi(z) = z - r(z), \quad (20)$$

where $r(z)$ denotes the residual nonlinearity measuring the deviation from the identity map. For these smooth rectifiers, $r(z)$ exhibits strong tail decay in the positive regime:

$$|r(z)| \leq C \exp(-\alpha z^2) \quad \text{for GELU}, \quad |r(z)| \leq C \exp(-\alpha z) \quad \text{for SiLU}, \quad (21)$$

for some constants $C, \alpha > 0$. As a consequence, $\phi'(z) \rightarrow 1$ and $\phi''(z) \rightarrow 0$ exponentially fast as $z \rightarrow +\infty$, implying that deviations from linearity are concentrated in a narrow neighborhood around $z \approx 0$.

In our setting, the distribution of pre-activations z is jointly shaped by three mechanisms: (i) ℓ_2 weight decay controls the operator norms and variance of the weights; (ii) magnitude-based unstructured pruning removes small-magnitude parameters, further reducing variance; (iii) entropy minimization enforces that neurons remain almost always in the same activation regime.

As shown in Sec. 3.2, the combined effect of these mechanisms is that pre-activations become increasingly concentrated and biased toward a single regime. In particular, in the almost-always-ON case, the distribution of z can be well approximated by

$$z \sim \mathcal{N}(\mu_z, \sigma_z^2), \quad \text{with } \mu_z \gg \sigma_z, \quad (22)$$

Using the decay properties of the residual nonlinearity $r(z)$ established above, the expected neuron-level approximation error can be bounded as

$$\mathbb{E}[\varepsilon(z)^2] = \mathbb{E}[r(z)^2] \leq \int r(z)^2 \mathcal{N}(z; \mu_z, \sigma_z^2) dz \leq C \exp(-\alpha \mu_z^2), \quad (23)$$

for GELU (and analogously exponential decay in μ_z for SiLU). Therefore, once a neuron enters a low-entropy (almost-always-ON) regime, the approximation error induced by replacing $\phi(z)$ with the identity decays exponentially in the mean pre-activation and rapidly becomes negligible in practice.

Let δ_ℓ denote the approximation error introduced by collapsing layer ℓ . The propagated error satisfies

$$\|\delta_{\ell+1}\| \leq \|W_{\ell+1}\| \|\delta_\ell\|. \quad (24)$$

Under ℓ_2 regularization, the operator norms $\|W_\ell\|$ remain controlled and empirically decrease with pruning, which also consistent with the observed reduction in loss landscape sharpness (Table. 3). Consequently, over k collapsed layers, the accumulated output error admits the bound

$$\|\delta_{\text{out}}\| \leq \sum_{\ell=1}^k \left(\prod_{j>\ell} \|W_j\| \right) \varepsilon_\ell, \quad (25)$$

which remains small since each ε_ℓ is exponentially suppressed. This explains why approximation errors introduced by collapsing multiple layers do not accumulate catastrophically in deep networks.

B Analysis for Rectifiers with More Intervals

Unstructured pruning can still induce layer collapse in networks where rectifiers have more intervals. Let us take the rectifier ReLU6 and apply NEPENTHE as an example. If $z_{l,i}^{\mathbf{x}}$ is the output of the i -th neuron inside the l -th layer from a given input \mathbf{x} of the dataset \mathcal{D} , the output $y_{l,i}^{\mathbf{x}}$ is:

$$y_{l,i}^{\mathbf{x}} = \min(\max(0, z_{l,i}^{\mathbf{x}}), 6), \quad (26)$$

There are two OFF states:

- $z_{l,i} \leq 0$. In this case, when employing a ReLU6, the output of the i -th neuron is always 0, we call this state OFF-. If a neuron has all its output in this state, this neuron can be simply pruned.
- $z_{l,i} \geq 6$. In this case, when employing a ReLU6, the output of the i -th neuron is always 6, we call this state OFF+. If a neuron has all its output in this state, this neuron can be replaced by a bias 6.

There is also one ON state:

- $0 \leq z_{l,i} \leq 6$. In this case, the output of the i -th neuron’s rectifier is always the same as its input, we call this state ON. If a neuron has all its output in this state, this neuron can in principle be absorbed by the following layer as there is no non-linearity between them anymore.

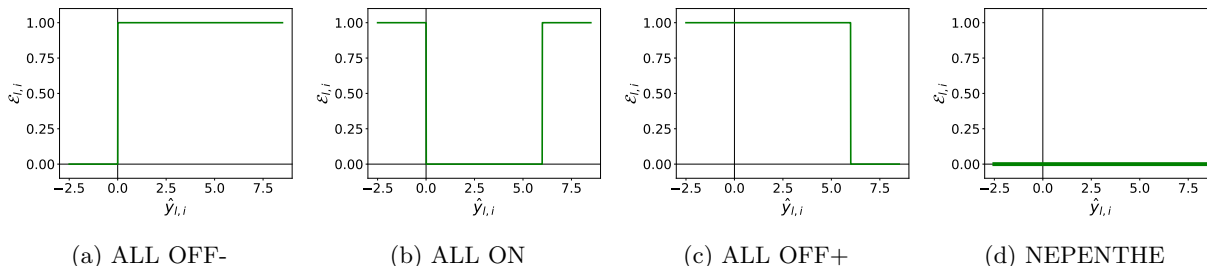


Figure 5: Error plot for the i -th neuron of the l -th ReLU6 activated layer as a function of the output average $\hat{y}_{l,i}$.

Fig. 5a shows how a neuron’s error varies with its average output $\hat{y}_{l,i}$ when substituting the rectifier with a null function, which means pushing all the neurons to always OFF- state. Fig. 5b shows the error of pushing all the neurons to always ON state by substituting the rectifier ψ_l by an identity function. Fig. 5c shows the error of pushing all the neurons to always OFF+ state by substituting the rectifier ψ_l by a bias 6. Each of the above methods produces obvious errors in some cases. As shown in Fig. 5d, NEPENTHE can remove layers without introducing any error. It appears that the phenomenon that unstructured pruning induces layer collapse also appears in networks with rectifiers with more intervals rather than two.

C Details on the Learning Strategies Employed

The implementation details used in this paper are presented here.

Like in the He et al. (2022)’s setup, for the ResNet-18 network, a modified version of the `torchvision` model is used: the first convolutional layer is set with a filter of size 3×3 and the max-pooling layer that follows has been eliminated to adapt ResNet-18 for CIFAR-10.

CIFAR-10 is augmented with per-channel normalization, random horizontal flipping, and random shifting by up to four pixels in any direction. For the datasets of DomainBed, the images are augmented with per-channel normalization, random horizontal flipping, random cropping, and resizing to 224. The brightness, contrast, saturation, and hue are also randomly affected with a factor fixed to 0.4. Tiny ImageNet is augmented

Table 11: Iterations (Iter.), Test performance (top-1), and the number of removed layers (Rem.) for MobileNet-V2 trained on CIFAR-10 and pruned by NEPENTHE with different ζ

(a) $\zeta = 0.05$			(b) $\zeta = 0.1$			(c) $\zeta = 0.25$		
Iter.	top-1	Rem.	Iter.	top-1	Rem.	Iter.	top-1	Rem.
1	93.42	1/35	1	93.55	1/35	1	94.12	1/35
3	93.56	2/35	3	93.14	2/35	3	10	18/35
7	93.36	5/35	7	93.26	7/35	7	-	-
9	93.54	7/35	9	92.78	9/35	9	-	-

Table 12: Table of the different employed learning strategies.

Model	Dataset	Epochs	Batch	Opt.	LR	β_1	β_2	ϵ
BERT	QNLI	3	32	AdamW	2e-5	0.9	0.999	1e-8
RoBERTa	QNLI	3	32	AdamW	2e-5	0.9	0.999	1e-8
BERT	RTE	3	32	AdamW	2e-5	0.9	0.999	1e-8
RoBERTa	RTE	3	32	AdamW	2e-5	0.9	0.999	1e-8
BERT	SST-2	3	32	AdamW	2e-5	0.9	0.999	1e-8
RoBERTa	SST-2	3	32	AdamW	2e-5	0.9	0.999	1e-8

with per-channel normalization and random horizontal flipping. ImageNet is augmented with per-channel normalization, random horizontal flipping, random cropping, and resizing to 224. The sequence length of SST-2, QNLI from Williams et al, and RTE is set to 128.

All weights from ReLU-activated layers are set as prunable for ResNet-18. For Swin-T, BERT, and RoBERTa, all weights from GELU-activated layers are prunable. while for MobileNetv2 all weights from ReLU6-activated layers are considered in the pruning. Neither biases nor batch normalization parameters are pruned.

ζ is a crucial parameter. As Table 11 shows, in our approach, since we utilize iterative pruning, if the sparse ratio is set too low, more iterations will be required to get removable layers (because we remove fewer parameters at a time). On the other hand, if the sparse ratio is set too high, the model’s performance will be destroyed quickly (because essential parameters are removed). Currently, we follow commonly used sparse ratios from unstructured pruning.

The training hyperparameters used in the Image classification experiments are presented in Table 13, hyperparameters used in the NLP experiments are presented in Table 12. We have performed our experiments on an NVIDIA A4500 GPU. Our code is attached to this supplementary material and will be publicly available upon acceptance of the article.

D More Detailed Results

D.1 Layer States for Models Trained on CIFAR-10

Fig. 6 shows the layers’ states for ResNet-18 trained on CIFAR-10 with different methods.

D.2 Experiments on More Architectures

Table 23 presents the results for ResNet-50, ResNet-152, and MobileNetV2-0.75 models trained on Cifar-10 dataset. Table 24 presents the results for ResNet-18 model trained on ImageNet dataset.

We also provide an ablation study on the three key components identifiable within NEPENTHE for Swin-T trained on Tiny-ImageNet. As shown in Table 14, each component contributes to the overall effectiveness of NEPENTHE.

Table 13: Table of the different employed learning strategies.

Model	Dataset	Epochs	Batch	Opt.	Mom.	LR	Milestones	Drop Factor	Weight Decay
ResNet-18	CIFAR-10	160	128	SGD	0.9	0.1	[80, 120]	0.1	1e-4
ResNet-50	CIFAR-10	160	128	SGD	0.9	0.1	[80, 120]	0.1	1e-4
ResNet-152	CIFAR-10	160	128	SGD	0.9	0.1	[80, 120]	0.1	1e-4
Swin-T	CIFAR-10	160	128	SGD	0.9	0.001	[80, 120]	0.1	1e-4
MobileNetv2	CIFAR-10	160	128	SGD	0.9	0.1	[80, 120]	0.1	1e-4
MobileNetV2-0.75	CIFAR-10	160	128	SGD	0.9	0.1	[80, 120]	0.1	1e-4
ResNet-18	PACS	30	16	SGD	0.9	0.001	[24]	0.1	5e-4
Swin-T	PACS	30	16	SGD	0.9	0.001	[24]	0.1	5e-4
MobileNetv2	PACS	30	16	SGD	0.9	0.001	[24]	0.1	5e-4
ResNet-18	VLCS	30	16	SGD	0.9	0.001	[24]	0.1	5e-4
Swin-T	VLCS	30	16	SGD	0.9	0.001	[24]	0.1	5e-4
MobileNetv2	VLCS	30	16	SGD	0.9	0.001	[24]	0.1	5e-4
ResNet-18	SVIRO	30	16	SGD	0.9	0.001	[24]	0.1	5e-4
Swin-T	SVIRO	30	16	SGD	0.9	0.001	[24]	0.1	5e-4
MobileNetv2	SVIRO	30	16	SGD	0.9	0.001	[24]	0.1	5e-4
ResNet-18	Tiny ImageNet	160	128	SGD	0.9	0.1	[80, 120]	0.1	1e-4
Swin-T	Tiny ImageNet	160	128	SGD	0.9	0.001	[80, 120]	0.1	1e-4
MobileNetv2	Tiny ImageNet	160	128	SGD	0.9	0.1	[80, 120]	0.1	1e-4
ResNet-18	ImageNet	90	128	SGD	0.9	0.1	[30, 90]	0.1	1e-4

Table 14: Ablation study on Swin-T trained on Tiny-ImageNet. Each component contributes to the effectiveness of NEPENTHE.

Entropy-based budget	Don't care state	Neurons selection	top-1	Rem.
			75.60	0/12
✓			71.48	1/12
✓	✓		71.54	1/12
✓	✓	✓	72.85	1/12

D.3 Potential Computational Savings

Table 15, 16, 17, 18, 19, 20, 21, 22 present the potential savings in terms of FLOPs, latency, and memory across different tasks trained by NEPENTHE and on different hardware. It appears that in general, the fewer layers the networks have, the lower the inference time.

Moreover, for unstructured sparsity, the FLOPs of the composed operator do not necessarily decrease, since multiplying two sparse matrices may introduce sparsity fill-in and yield a denser effective operator. However, this concern does not apply to the computational setting considered in our work, and we clarify the distinction here.

Our statement that a linearized layer can be “absorbed by the following layer” is an *algebraic* statement about function composition:

$$W_{l+1}(W_l x) = (W_{l+1}W_l)x. \quad (27)$$

Importantly, NEPENTHE does not rely on performing runtime multiplication of two unstructured sparse matrices. Once a layer reaches (near-)zero entropy and is deemed linearizable, it is removed entirely from the computational graph, and the model is recompiled with reduced depth. This is a layer removal operation, not a sparse-sparse fusion executed at inference time.

We do not claim that the product $W_{l+1}W_l$ preserves the sparsity pattern of the original matrices. Indeed, sparsity fill-in is expected in general. However, our method does not require sparsity preservation in the merged operator, because the primary source of computational savings in our work is depth reduction, i.e., shortening the critical path of forward propagation, rather than exploiting sparse matrix kernels.

The reductions reported in our efficiency evaluation are based on actual measured inference time, memory usage, and energy consumption, rather than on idealized sparse FLOP counts. On modern GPUs, unstructured

Table 15: MFLOPs, Inference time [ms], Memory usage [MBs], and Energy consumption [mJ] of ResNet-18 on CIFAR-10 across different hardware platforms.

Hardware	Rem.	MFLOPs	Inference time [ms]	Mem.usage [MBs]	top-1
NVIDIA A4500	0/17	725.47	3.32	230	91.66
	3/17	231.79	2.96	170	92.55
RTX 2080	0/17	725.47	3.32	230	91.66
	3/17	231.79	2.96	170	92.55
RTX 4000	0/17	725.47	4.52	241	91.66
	3/17	231.79	3.94	212	92.55
Jetson Nano	0/17	725.47	8.52	241	91.66
	3/17	231.79	7.38	178	92.55

Table 16: MFLOPs, Inference time [ms], Memory usage [MBs], and Energy consumption [mJ] of ResNet-18 on Tiny-ImageNet across different hardware platforms.

Hardware	Rem.	MFLOPs	Inference time [ms]	Mem.usage [MBs]	top-1
NVIDIA A4500	0/17	7292.87	3.56	227	41.44
	2/17	7618.77	3.24	225	41.42
RTX 2080	0/17	7292.87	4.62	227	41.44
	2/17	7618.77	4.21	225	41.42
NVIDIA A4000	0/17	7292.87	4.73	228	41.44
	2/17	7618.77	4.27	225	41.42
Jetson Nano	0/17	7292.87	12.06	228	41.44
	2/17	7618.77	11.87	226	41.42

sparsity alone often yields limited speedups due to kernel launch overheads and memory access patterns. In contrast, reducing the number of layers directly reduces (i) kernel invocations, (ii) synchronization points, and (iii) activation storage and memory traffic. Therefore, even if the merged linear operator were dense, removing an entire layer can still lead to tangible performance gains, as empirically demonstrated.

D.4 Trend of Layer’s Entropy and Training Time

Tables 25, 26, 27, 28, 29, 30, 31, 32, 33, 34, 35, 36, 37, 38, 39, 41, 41, 42, 43, 44, 45, present the entropy trends in the six layers exhibiting the lowest entropy and the training time, for all the unstructured pruning and NEPENTHE setups. This illustrates that while unstructured pruning inherently reduces the entropy of certain layers, as detailed in Section 4.2, it lacks the capability to entirely eliminate any specific layer. In contrast, our methodology, NEPENTHE, aims to push all the encoded information from layers with low entropy to those with already high entropy. This strategy enables the removal of zero-entropy layers.

Table 17: MFLOPs, Inference time [ms], Memory usage [MBs], and Energy consumption [mJ] of ResNet-18 on PACS across different hardware platforms.

Hardware	Rem.	MFLOPs	Inference time [ms]	Mem.usage [MBs]	top-1
NVIDIA A4500	0/17	7292.67	3.58	248	94.70
	3/17	6736.15	3.04	181	90.10
RTX 2080	0/17	7292.67	4.54	248	94.70
	3/17	6736.15	4.00	181	90.10
NVIDIA A4000	0/17	7292.67	4.61	248	94.70
	3/17	6736.15	4.09	182	90.10
Jetson Nano	0/17	7292.67	12.00	248	94.70
	3/17	6736.15	11.04	181	90.10

Table 18: MFLOPs, Inference time [ms], Memory usage [MBs], and Energy consumption [mJ] of ResNet-18 on VLCS across different hardware platforms.

Hardware	Rem.	MFLOPs	Inference time [ms]	Mem.usage [MBs]	top-1
NVIDIA A4500	0/17	7292.67	3.56	285	80.89
	2/17	6760.27	3.05	258	78.38
RTX 2080	0/17	7292.67	4.58	285	80.89
	2/17	6760.27	4.21	257	78.38
NVIDIA A4000	0/17	7292.67	4.66	286	80.89
	2/17	6760.27	4.17	258	78.38
Jetson Nano	0/17	7292.67	12.00	285	80.89
	2/17	6760.27	7.75	258	78.38

Table 19: MFLOPs, Inference time [ms], Memory usage [MBs], and Energy consumption [mJ] of Swin-T on CIFAR-10 across different hardware platforms.

Hardware	Rem.	MFLOPs	Inference time [ms]	Mem.usage [MBs]	top-1
NVIDIA A4500	0/12	1041.34	7.79	245	91.54
	2/12	1020.11	7.71	79	92.29
RTX 2080	0/12	1041.34	3.32	230	91.54
	2/12	1020.11	2.96	120	92.29
RTX 4000	0/12	1041.34	4.52	241	91.54
	2/12	1020.11	3.94	212	92.29
Jetson Nano	0/12	1041.34	8.52	241	91.54
	2/12	1020.11	7.38	128	92.29

Table 20: MFLOPs, Inference time [ms], Memory usage [MBs], and Energy consumption [mJ] of Swin-T on Tiny-ImageNet across different hardware platforms.

Hardware	Rem.	MFLOPs	Inference time [ms]	Mem.usage [MBs]	top-1
NVIDIA A4500	0/12	7546.87	3.56	155	75.60
	1/12	7511.50	3.24	100	72.58
RTX 2080	0/12	7546.87	4.62	245	75.60
	1/12	7511.50	4.21	80	72.58
NVIDIA A4000	0/12	7546.87	4.73	155	75.60
	1/12	7511.50	4.27	100	72.58
Jetson Nano	0/12	7546.87	12.06	156	75.60
	1/12	7511.50	11.87	100	72.58

Table 21: MFLOPs, Inference time [ms], Memory usage [MBs], and Energy consumption [mJ] of Swin-T on PACS across different hardware platforms.

Hardware	Rem.	MFLOPs	Inference time [ms]	Mem.usage [MBs]	top-1
NVIDIA A4500	0/12	8989.52	9.47	212	97.10
	2/12	8177.89	9.27	115	95.10
RTX 2080	0/12	8989.52	15.09	212	97.10
	2/12	8177.89	14.92	114	95.10
NVIDIA A4000	0/12	8989.52	16.02	209	97.10
	2/12	8177.89	15.76	115	95.10
Jetson Nano	0/12	8989.52	38.71	212	97.10
	2/12	8177.89	38.93	115	95.10

Table 22: MFLOPs, Inference time [ms], Memory usage [MBs], and Energy consumption [mJ] of Swin-T on VLCS across different hardware platforms.

Hardware	Rem.	MFLOPs	Inference time [ms]	Mem.usage [MBs]	top-1
NVIDIA A4500	0/12	8989.48	9.48	194	80.89
	1/12	8582.50	9.34	118	78.38
RTX 2080	0/12	8989.48	15.09	194	80.89
	1/12	8582.50	14.94	120	78.38
NVIDIA A4000	0/12	8989.48	16.00	194	80.89
	1/12	8582.50	15.85	120	78.38
Jetson Nano	0/12	8989.48	39.61	195	80.89
	1/12	8582.50	38.93	118	78.38

Table 23: Test performance (top-1) and the number of removed layers (Rem.) for ResNet-50, ResNet-152, and MobileNetV2-0.75 models trained on CIFAR-10.

Dataset	Approach	ResNet-50		ResNet-152		MobileNetV2-0.75	
		Top-1	Rem.	Top-1	Rem.	Top-1	Rem.
CIFAR-10	Dense	87.37	0/49	85.61	0/151	85.17	0/35
	NEPENTHE	89.06	16/49	89.20	82/151	87.06	12/35

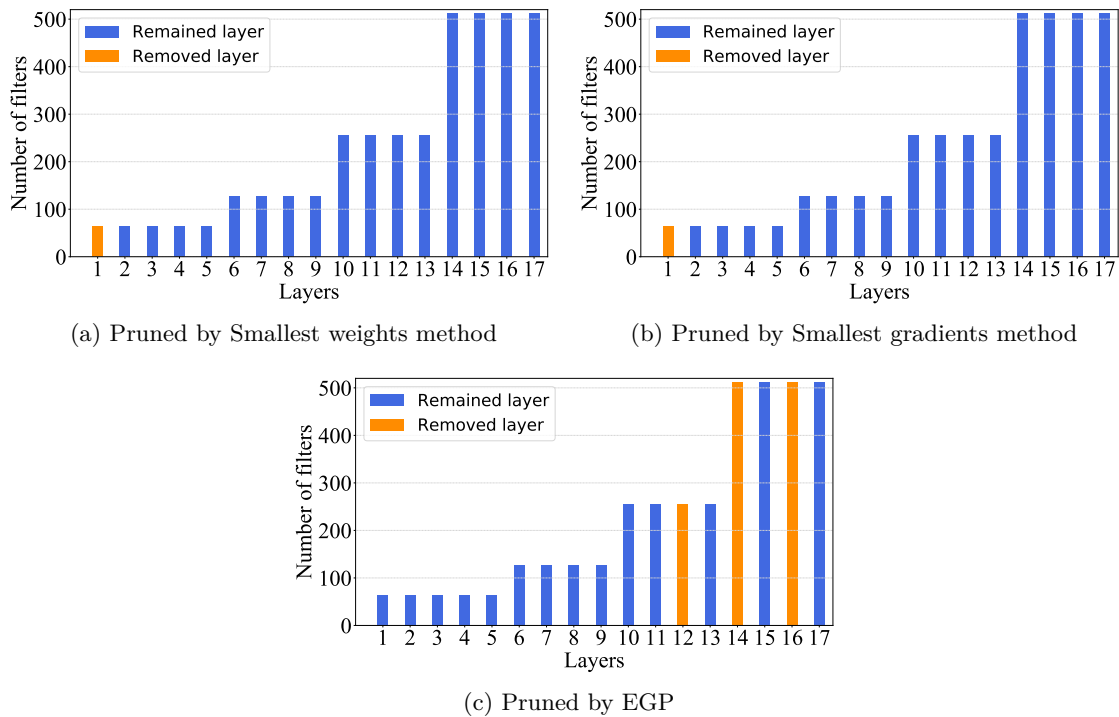


Figure 6: Layer states for ResNet-18 trained on CIFAR-10 with different methods.

Table 24: Test performance (top-1) and the number of removed layers (Rem.) for Resnet-18 trained on Imagenet.

Dataset	Approach	ResNet-18	
		top-1	Rem.
ImageNet	Dense model	68.20	0/17
	IMP (low prune)	68.38	0/17
	IMP (mid prune)	67.88	0/17
	IMP (high prune)	66.63	0/17
	NEPENTHE (low prune)	66.17	0/17
	NEPENTHE (mid prune)	62.74	1/17
	NEPENTHE (high prune)	62.15	3/17

Table 25: Test performance (top-1), bottom six layer’s entropies $\hat{\mathcal{H}}$ and the number of removed layers (Rem.) for ResNet-18 on CIFAR-10.

Approach	$\hat{\mathcal{H}}_1$	$\hat{\mathcal{H}}_2$	$\hat{\mathcal{H}}_3$	$\hat{\mathcal{H}}_4$	$\hat{\mathcal{H}}_5$	$\hat{\mathcal{H}}_6$	top-1	Rem.	Time
Dense model	0.647	0.680	0.728	0.785	0.791	0.797	91.66	0/17	0h48
IMP(iter #1)	0.585	0.650	0.699	0.725	0.767	0.778	92.29	0/17	1h36
IMP(iter #2)	0.506	0.580	0.647	0.654	0.700	0.722	92.25	0/17	2h24
IMP(iter #3)	0.256	0.623	0.658	0.672	0.682	0.737	92.46	0/17	3h12
IMP(iter #4)	0.192	0.660	0.667	0.676	0.698	0.763	92.27	0/17	4h00
IMP(iter #5)	0.136	0.589	0.648	0.727	0.728	0.791	92.44	0/17	4h48
IMP(iter #6)	0.093	0.447	0.640	0.650	0.764	0.765	91.89	0/17	5h36
IMP(iter #7)	0.055	0.335	0.487	0.592	0.640	0.775	91.66	0/17	6h24
NEPENTHE(iter #1)	0	0.168	0.581	0.654	0.681	0.714	92.25	1/17	1h37
NEPENTHE(iter #2)	0	0.076	0.615	0.619	0.633	0.644	92.60	1/17	2h26
NEPENTHE(iter #3)	0	0	0	0.121	0.139	0.642	92.55	3/17	3h15
NEPENTHE(iter #4)	0	0	0	0.003	0.242	0.320	91.93	3/17	4h04
NEPENTHE(iter #5)	0	0	0	0	0	0.114	89.30	5/17	4h53
NEPENTHE(iter #6)	0	0	0	0	0	0.019	89.43	5/17	5h42
NEPENTHE(iter #7)	0	0	0	0	0	0	83.42	6/17	6h31

Table 26: Test performance (top-1), bottom six layer’s entropies $\hat{\mathcal{H}}$ and the number of removed layers (Rem.) for Swin-T on CIFAR-10.

Approach	$\hat{\mathcal{H}}_1$	$\hat{\mathcal{H}}_2$	$\hat{\mathcal{H}}_3$	$\hat{\mathcal{H}}_4$	$\hat{\mathcal{H}}_5$	$\hat{\mathcal{H}}_6$	top-1	Rem.	Time
Dense model	0.03	0.054	0.382	0.394	0.394	0.44	91.54	0/12	1h53
IMP(iter #1)	0.03	0.055	0.383	0.397	0.398	0.444	91.73	0/12	3h46
IMP(iter #2)	0.031	0.057	0.382	0.392	0.399	0.443	91.80	0/12	5h39
IMP(iter #3)	0.034	0.063	0.375	0.383	0.393	0.438	91.43	0/12	7h32
IMP(iter #4)	0.036	0.072	0.365	0.379	0.382	0.426	91.46	0/12	9h25
IMP(iter #5)	0.041	0.080	0.349	0.361	0.369	0.409	91.27	0/12	11h18
IMP(iter #6)	0.048	0.096	0.334	0.343	0.350	0.386	91.05	0/12	13h11
IMP(iter #7)	0.055	0.113	0.31	0.325	0.327	0.355	90.53	0/12	15h04
NEPENTHE(iter #1)	0.001	0.215	0.385	0.397	0.407	0.443	91.77	0/12	3h48
NEPENTHE(iter #2)	0.001	0.219	0.387	0.399	0.409	0.445	92.06	0/12	5h45
NEPENTHE(iter #3)	0.001	0.254	0.380	0.395	0.405	0.440	92.08	0/12	7h38
NEPENTHE(iter #4)	0.001	0.001	0.377	0.388	0.404	0.433	92.31	0/12	9h33
NEPENTHE(iter #5)	0	0	0.363	0.373	0.406	0.423	92.29	2/12	11h28
NEPENTHE(iter #6)	0	0	0.344	0.359	0.407	0.412	92.21	2/12	13h23
NEPENTHE(iter #7)	0	0	0.287	0.317	0.405	0.405	92.11	2/12	15h18

Table 27: Test performance (top-1), bottom six layer’s entropies $\widehat{\mathcal{H}}$ and the number of removed layers (Rem.) for MobileNetv2 on CIFAR-10.

Approach	$\widehat{\mathcal{H}}_1$	$\widehat{\mathcal{H}}_2$	$\widehat{\mathcal{H}}_3$	$\widehat{\mathcal{H}}_4$	$\widehat{\mathcal{H}}_5$	$\widehat{\mathcal{H}}_6$	top-1	Rem.	Time
Dense model	0.386	0.474	0.486	0.504	0.528	0.544	93.68	0/35	0h43
IMP(iter #1)	0.186	0.206	0.233	0.241	0.249	0.260	94.07	0/35	1h26
IMP(iter #2)	0.116	0.117	0.153	0.167	0.167	0.168	93.67	0/35	2h09
IMP(iter #3)	0.082	0.084	0.111	0.119	0.119	0.125	93.83	0/35	2h52
IMP(iter #4)	0.063	0.066	0.090	0.094	0.095	0.101	93.32	0/35	3h35
IMP(iter #5)	0.056	0.057	0.074	0.075	0.086	0.088	93.26	0/35	4h18
IMP(iter #6)	0.050	0.050	0.065	0.067	0.071	0.076	93.47	0/35	5h01
IMP(iter #7)	0.046	0.047	0.059	0.060	0.061	0.064	93.50	0/35	5h44
NEPENTHE(iter #1)	0	0.198	0.229	0.232	0.244	0.248	93.55	1/35	1h27
NEPENTHE(iter #2)	0	0.109	0.127	0.138	0.139	0.149	93.42	1/35	2h11
NEPENTHE(iter #3)	0	0.082	0.085	0.103	0.106	0.107	93.14	1/35	2h55
NEPENTHE(iter #4)	0	0	0.063	0.065	0.074	0.076	93.25	2/35	3h39
NEPENTHE(iter #5)	0	0	0.064	0.067	0.049	0.051	93.37	4/35	4h23
NEPENTHE(iter #6)	0	0	0	0	0	0.042	93.15	5/35	5h07
NEPENTHE(iter #7)	0	0	0	0	0	0	93.26	7/35	5h51

Table 28: Test performance (top-1), bottom six layer’s entropies $\widehat{\mathcal{H}}$ and the number of removed layers (Rem.) for ResNet-18 on Tiny ImageNet.

Approach	$\widehat{\mathcal{H}}_1$	$\widehat{\mathcal{H}}_2$	$\widehat{\mathcal{H}}_3$	$\widehat{\mathcal{H}}_4$	$\widehat{\mathcal{H}}_5$	$\widehat{\mathcal{H}}_6$	top-1	Rem.	Time
Dense model	0.471	0.500	0.592	0.625	0.627	0.783	41.44	0/17	2h15
IMP(iter #1)	0.470	0.540	0.621	0.662	0.666	0.780	42.24	0/17	4h30
IMP(iter #2)	0.461	0.621	0.637	0.697	0.726	0.781	42.12	0/17	6h45
IMP(iter #3)	0.487	0.643	0.735	0.736	0.776	0.779	42.10	0/17	9h00
IMP(iter #4)	0.488	0.643	0.760	0.783	0.831	0.831	41.18	0/17	11h15
IMP(iter #5)	0.482	0.605	0.727	0.839	0.845	0.872	39.92	0/17	13h30
IMP(iter #6)	0.469	0.585	0.690	0.814	0.834	0.834	37.16	0/17	15h45
IMP(iter #7)	0.464	0.544	0.641	0.661	0.725	0.741	39.14	0/17	18h00
NEPENTHE(iter #1)	0	0	0.063	0.559	0.633	0.699	41.42	2/17	4h33
NEPENTHE(iter #2)	0	0	0	0	0	0.129	39.56	5/17	6h51
NEPENTHE(iter #3)	0	0	0	0	0	0.169	40.00	5/17	9h09
NEPENTHE(iter #4)	0	0	0	0	0	0.109	39.40	5/17	11h27
NEPENTHE(iter #5)	0	0	0	0	0	0.107	38.58	5/17	13h45
NEPENTHE(iter #6)	0	0	0	0	0	0.125	37.34	5/17	16h03
NEPENTHE(iter #7)	0	0	0	0	0	0.138	35.80	5/17	18h21

Table 29: Test performance (top-1), bottom six layer’s entropies $\widehat{\mathcal{H}}$ and the number of removed layers (Rem.) for Swin-T on Tiny ImageNet.

Approach	$\widehat{\mathcal{H}}_1$	$\widehat{\mathcal{H}}_2$	$\widehat{\mathcal{H}}_3$	$\widehat{\mathcal{H}}_4$	$\widehat{\mathcal{H}}_5$	$\widehat{\mathcal{H}}_6$	top-1	Rem.	Time
Dense model	0.067	0.133	0.38	0.388	0.395	0.411	75.60	0/12	5h41
IMP(iter #1)	0.069	0.131	0.370	0.373	0.384	0.399	75.86	0/12	11h22
IMP(iter #2)	0.073	0.133	0.355	0.356	0.367	0.380	75.26	0/12	17h03
IMP(iter #3)	0.080	0.143	0.335	0.336	0.346	0.357	73.60	0/12	22h44
IMP(iter #4)	0.089	0.156	0.313	0.314	0.319	0.330	72.32	0/12	28h25
IMP(iter #5)	0.096	0.169	0.291	0.291	0.295	0.309	70.90	0/12	34h06
IMP(iter #6)	0.102	0.184	0.268	0.269	0.275	0.294	69.80	0/12	39h47
IMP(iter #7)	0.104	0.193	0.249	0.255	0.266	0.289	67.56	0/12	45h28
NEPENTHE(iter #1)	0	0.139	0.370	0.377	0.392	0.394	72.58	1/12	11h27
NEPENTHE(iter #2)	0	0.143	0.150	0.183	0.195	0.381	71.02	1/12	17h13
NEPENTHE(iter #3)	0	0.143	0.158	0.183	0.192	0.269	70.76	1/12	22h59
NEPENTHE(iter #4)	0	0.133	0.137	0.165	0.178	0.187	70.12	1/12	28h45
NEPENTHE(iter #5)	0	0.128	0.132	0.172	0.173	0.180	69.68	1/12	34h36
NEPENTHE(iter #6)	0	0.124	0.129	0.164	0.174	0.176	70.06	1/12	39h17
NEPENTHE(iter #7)	0	0.123	0.128	0.160	0.170	0.180	69.42	1/12	46h03

Table 30: Test performance (top-1), bottom six layer’s entropies $\widehat{\mathcal{H}}$ and the number of removed layers (Rem.) for MobileNetv2 on Tiny ImageNet.

Approach	$\widehat{\mathcal{H}}_1$	$\widehat{\mathcal{H}}_2$	$\widehat{\mathcal{H}}_3$	$\widehat{\mathcal{H}}_4$	$\widehat{\mathcal{H}}_5$	$\widehat{\mathcal{H}}_6$	top-1	Rem.	Time
Dense model	0.076	0.112	0.131	0.133	0.153	0.154	45.860	0/35	1h47
IMP(iter #1)	0.036	0.039	0.039	0.045	0.048	0.054	45.84	0/35	3h34
IMP(iter #2)	0.025	0.026	0.031	0.035	0.037	0.037	47.10	0/35	5h21
IMP(iter #3)	0.018	0.021	0.030	0.030	0.031	0.031	47.740	0/35	7h08
IMP(iter #4)	0.016	0.017	0.028	0.028	0.030	0.030	46.800	0/35	8h55
IMP(iter #5)	0.013	0.016	0.025	0.025	0.028	0.029	47.560	0/35	10h42
IMP(iter #6)	0.008	0.011	0.022	0.023	0.028	0.028	47.580	0/35	12h29
IMP(iter #7)	0.007	0.01	0.022	0.023	0.028	0.029	47.440	0/35	14h16
NEPENTHE(iter #1)	0.001	0.004	0.095	0.096	0.098	0.110	46.70	0/35	3h37
NEPENTHE(iter #2)	0	0.003	0.058	0.064	0.071	0.073	47.22	1/35	5h27
NEPENTHE(iter #3)	0	0	0	0	0	0	47.26	6/35	7h17
NEPENTHE(iter #4)	0	0	0	0	0	0	47.82	9/35	9h07
NEPENTHE(iter #5)	0	0	0	0	0	0	47.92	12/35	10h57
NEPENTHE(iter #6)	0	0	0	0	0	0	0.50	34/35	12h37

Table 31: Test performance (top-1), bottom six layer’s entropies $\hat{\mathcal{H}}$ and the number of removed layers (Rem.) for ResNet-18 on PACS.

Approach	$\hat{\mathcal{H}}_1$	$\hat{\mathcal{H}}_2$	$\hat{\mathcal{H}}_3$	$\hat{\mathcal{H}}_4$	$\hat{\mathcal{H}}_5$	$\hat{\mathcal{H}}_6$	top-1	Rem.	Time
Dense model	0.332	0.439	0.602	0.667	0.686	0.687	94.70	0/17	0h46
IMP(iter #1)	0.331	0.423	0.608	0.669	0.688	0.688	95.40	0/17	1h31
IMP(iter #2)	0.319	0.429	0.602	0.668	0.670	0.683	95.30	0/17	2h17
IMP(iter #3)	0.324	0.419	0.607	0.631	0.682	0.682	94.60	0/17	3h03
IMP(iter #4)	0.318	0.441	0.613	0.613	0.661	0.688	95.10	0/17	3h49
IMP(iter #5)	0.300	0.452	0.587	0.621	0.636	0.694	94.00	0/17	4h35
IMP(iter #6)	0.285	0.458	0.533	0.643	0.647	0.694	92.30	0/17	5h21
IMP(iter #7)	0.280	0.418	0.479	0.584	0.646	0.657	90.80	0/17	6h07
NEPENTHE(iter #1)	0.129	0.430	0.482	0.634	0.668	0.669	94.20	0/17	1h32
NEPENTHE(iter #2)	0	0.041	0.091	0.482	0.596	0.596	92.40	1/17	2h19
NEPENTHE(iter #3)	0	0.030	0.066	0.527	0.559	0.599	93.00	1/17	3h06
NEPENTHE(iter #4)	0	0	0.033	0.067	0.422	0.565	90.40	2/17	3h53
NEPENTHE(iter #5)	0	0	0.032	0.061	0.084	0.217	89.50	2/17	4h40
NEPENTHE(iter #6)	0	0	0	0.001	0.002	0.028	90.10	3/17	5h27
NEPENTHE(iter #7)	0	0	0	0.002	0.002	0.040	86.30	3/17	6h14

Table 32: Test performance (top-1), bottom six layer’s entropies $\hat{\mathcal{H}}$ and the number of removed layers (Rem.) for Swin-T on PACS.

Approach	$\hat{\mathcal{H}}_1$	$\hat{\mathcal{H}}_2$	$\hat{\mathcal{H}}_3$	$\hat{\mathcal{H}}_4$	$\hat{\mathcal{H}}_5$	$\hat{\mathcal{H}}_6$	top-1	Rem.	Time
Dense model	0.057	0.184	0.344	0.362	0.380	0.381	97.10	0/12	0h57
IMP(iter #1)	0.060	0.204	0.349	0.362	0.382	0.389	96.60	0/12	1h54
IMP(iter #2)	0.067	0.214	0.357	0.370	0.383	0.388	96.20	0/12	2h51
IMP(iter #3)	0.081	0.245	0.362	0.366	0.375	0.378	96.00	0/12	3h48
IMP(iter #4)	0.095	0.269	0.352	0.353	0.355	0.372	96.60	0/12	4h45
IMP(iter #5)	0.110	0.303	0.314	0.335	0.339	0.341	95.00	0/12	5h42
IMP(iter #6)	0.113	0.278	0.306	0.318	0.321	0.329	94.60	0/12	6h39
IMP(iter #7)	0.101	0.232	0.269	0.284	0.293	0.298	93.90	0/12	7h36
NEPENTHE(iter #1)	0.086	0.240	0.344	0.376	0.376	0.403	96.90	0/12	1h55
NEPENTHE(iter #2)	0.001	0.369	0.372	0.383	0.398	0.416	96.50	0/12	2h53
NEPENTHE(iter #3)	0.001	0.368	0.383	0.385	0.390	0.406	95.90	0/12	3h51
NEPENTHE(iter #4)	0.001	0.360	0.369	0.369	0.392	0.394	96.30	0/12	4h49
NEPENTHE(iter #5)	0	0	0.001	0.335	0.359	0.366	95.10	2/12	5h47
NEPENTHE(iter #6)	0	0	0.107	0.298	0.348	0.349	94.60	2/12	6h45
NEPENTHE(iter #7)	0	0	0.001	0.001	0.161	0.232	93.30	2/12	7h43

Table 33: Test performance (top-1), bottom six layer’s entropies $\widehat{\mathcal{H}}$ and the number of removed layers (Rem.) for MobileNetv2 on PACS.

Approach	$\widehat{\mathcal{H}}_1$	$\widehat{\mathcal{H}}_2$	$\widehat{\mathcal{H}}_3$	$\widehat{\mathcal{H}}_4$	$\widehat{\mathcal{H}}_5$	$\widehat{\mathcal{H}}_6$	top-1	Rem.	Time
Dense model	0.207	0.291	0.324	0.372	0.463	0.471	93.20	0/35	0h34
IMP(iter #1)	0.218	0.263	0.284	0.390	0.457	0.467	95.70	0/35	1h09
IMP(iter #2)	0.216	0.235	0.257	0.373	0.453	0.462	95.50	0/35	1h44
IMP(iter #3)	0.224	0.244	0.252	0.403	0.464	0.478	95.40	0/35	2h19
IMP(iter #4)	0.222	0.229	0.241	0.386	0.459	0.476	95.70	0/35	2h54
IMP(iter #5)	0.212	0.223	0.233	0.397	0.464	0.47	95.60	0/35	3h29
IMP(iter #6)	0.196	0.212	0.237	0.405	0.470	0.485	96.20	0/35	4h04
IMP(iter #7)	0.170	0.207	0.234	0.412	0.468	0.472	95.40	0/35	4h39
NEPENTHE(iter #1)	0.119	0.139	0.151	0.192	0.200	0.225	93.30	0/35	1h10
NEPENTHE(iter #2)	0.093	0.128	0.129	0.130	0.135	0.165	93.20	0/35	1h46
NEPENTHE(iter #3)	0.077	0.093	0.112	0.125	0.140	0.141	92.50	0/35	2h22
NEPENTHE(iter #4)	0	0.076	0.083	0.105	0.106	0.116	92.20	1/35	2h58
NEPENTHE(iter #5)	0	0.054	0.068	0.096	0.097	0.115	89.70	1/35	3h34
NEPENTHE(iter #6)	0	0.014	0.016	0.036	0.050	0.051	89.00	1/35	4h10
NEPENTHE(iter #7)	0	0.004	0.008	0.023	0.027	0.034	88.70	1/35	4h46

Table 34: Test performance (top-1), bottom six layer’s entropies $\widehat{\mathcal{H}}$ and the number of removed layers (Rem.) for ResNet-18 on VLCS.

Approach	$\widehat{\mathcal{H}}_1$	$\widehat{\mathcal{H}}_2$	$\widehat{\mathcal{H}}_3$	$\widehat{\mathcal{H}}_4$	$\widehat{\mathcal{H}}_5$	$\widehat{\mathcal{H}}_6$	top-1	Rem.	Time
Dense model	0.382	0.457	0.647	0.676	0.681	0.698	80.89	0/17	3h49
IMP(iter #1)	0.387	0.471	0.647	0.679	0.681	0.703	82.76	0/17	8h37
IMP(iter #2)	0.392	0.476	0.644	0.654	0.69	0.703	82.01	0/17	13h06
IMP(iter #3)	0.378	0.474	0.620	0.658	0.707	0.707	82.01	0/17	17h15
IMP(iter #4)	0.391	0.491	0.595	0.672	0.711	0.726	80.15	0/17	22h24
IMP(iter #5)	0.372	0.479	0.571	0.665	0.716	0.739	79.31	0/17	27h13
IMP(iter #6)	0.383	0.519	0.531	0.699	0.721	0.750	78.84	0/17	31h22
IMP(iter #7)	0.357	0.409	0.502	0.64	0.707	0.712	74.09	0/17	35h11
NEPENTHE(iter #1)	0.001	0.453	0.497	0.651	0.676	0.680	78.99	0/17	8h44
NEPENTHE(iter #2)	0	0	0.001	0.508	0.516	0.619	78.38	2/17	13h20
NEPENTHE(iter #3)	0	0	0	0	0.518	0.553	76.98	4/17	17h36
NEPENTHE(iter #4)	0	0	0	0	0.516	0.574	78.66	4/17	22h52
NEPENTHE(iter #5)	0	0	0	0	0	0	76.05	6/17	27h48
NEPENTHE(iter #6)	0	0	0	0	0	0	74.28	6/17	32h04
NEPENTHE(iter #7)	0	0	0	0	0	0	74.37	6/17	36h01

Table 35: Test performance (top-1), bottom six layer’s entropies $\widehat{\mathcal{H}}$ and the number of removed layers (Rem.) for Swin-T on VLCS.

Approach	$\widehat{\mathcal{H}}_1$	$\widehat{\mathcal{H}}_2$	$\widehat{\mathcal{H}}_3$	$\widehat{\mathcal{H}}_4$	$\widehat{\mathcal{H}}_5$	$\widehat{\mathcal{H}}_6$	top-1	Rem.	Time
Dense model	0.070	0.175	0.373	0.385	0.414	0.427	86.58	0/12	2h22
IMP(iter #1)	0.078	0.179	0.391	0.402	0.421	0.433	84.72	0/12	4h45
IMP(iter #2)	0.093	0.195	0.387	0.403	0.416	0.419	85.65	0/12	8h08
IMP(iter #3)	0.102	0.224	0.388	0.411	0.424	0.424	84.34	0/12	11h31
IMP(iter #4)	0.122	0.236	0.395	0.402	0.415	0.418	84.06	0/12	14h54
IMP(iter #5)	0.140	0.261	0.369	0.394	0.404	0.412	82.01	0/12	18h56
IMP(iter #6)	0.141	0.292	0.331	0.387	0.390	0.393	81.36	0/12	22h38
IMP(iter #7)	0.139	0.277	0.304	0.370	0.373	0.374	80.06	0/12	26h20
NEPENTHE(iter #1)	0.121	0.187	0.400	0.402	0.430	0.437	85.46	0/12	4h57
NEPENTHE(iter #2)	0.132	0.225	0.403	0.406	0.428	0.438	85.09	0/12	8h26
NEPENTHE(iter #3)	0	0.411	0.413	0.432	0.437	0.457	85.27	1/12	11h55
NEPENTHE(iter #4)	0	0.409	0.420	0.441	0.446	0.463	83.88	1/12	15h18
NEPENTHE(iter #5)	0	0.406	0.409	0.428	0.434	0.469	81.73	1/12	19h28
NEPENTHE(iter #6)	0	0.318	0.383	0.398	0.413	0.469	81.55	1/12	23h20
NEPENTHE(iter #7)	0	0.001	0.304	0.369	0.374	0.475	79.22	1/12	27h08

Table 36: Test performance (top-1), bottom six layer’s entropies $\widehat{\mathcal{H}}$ and the number of removed layers (Rem.) for MobileNetv2 on VLCS.

Approach	$\widehat{\mathcal{H}}_1$	$\widehat{\mathcal{H}}_2$	$\widehat{\mathcal{H}}_3$	$\widehat{\mathcal{H}}_4$	$\widehat{\mathcal{H}}_5$	$\widehat{\mathcal{H}}_6$	top-1	Rem.	Time
Dense model	0.257	0.353	0.46	0.513	0.514	0.572	81.83	0/35	3h00
IMP(iter #1)	0.270	0.292	0.490	0.503	0.533	0.573	80.80	0/35	6h01
IMP(iter #2)	0.261	0.263	0.507	0.524	0.528	0.562	81.64	0/35	9h01
IMP(iter #3)	0.269	0.271	0.496	0.501	0.536	0.573	80.43	0/35	12h02
IMP(iter #4)	0.258	0.258	0.491	0.521	0.550	0.579	79.59	0/35	15h03
IMP(iter #5)	0.264	0.271	0.474	0.540	0.545	0.589	79.96	0/35	18h03
IMP(iter #6)	0.268	0.277	0.468	0.547	0.549	0.585	80.80	0/35	21h04
IMP(iter #7)	0.273	0.279	0.470	0.524	0.554	0.592	80.43	0/35	24h05
NEPENTHE(iter #1)	0.184	0.249	0.342	0.505	0.534	0.581	81.08	0/35	6h04
NEPENTHE(iter #2)	0.001	0.077	0.251	0.345	0.417	0.500	80.52	0/35	9h07
NEPENTHE(iter #3)	0	0.002	0.005	0.260	0.354	0.488	78.84	1/35	12h11
NEPENTHE(iter #4)	0	0.001	0.040	0.261	0.363	0.527	77.91	1/35	15h15
NEPENTHE(iter #5)	0	0	0.001	0.274	0.366	0.523	80.06	2/35	18h18
NEPENTHE(iter #6)	0	0	0.001	0.26	0.351	0.485	79.31	2/35	21h22

Table 37: Test performance (top-1), bottom six layer’s entropies $\widehat{\mathcal{H}}$ and the number of removed layers (Rem.) for ResNet-18 on SVIRO.

Approach	$\widehat{\mathcal{H}}_1$	$\widehat{\mathcal{H}}_2$	$\widehat{\mathcal{H}}_3$	$\widehat{\mathcal{H}}_4$	$\widehat{\mathcal{H}}_5$	$\widehat{\mathcal{H}}_6$	top-1	Rem.	Time
Dense model	0.009	0.446	0.631	0.685	0.693	0.707	99.93	0/17	7h03
IMP(iter #1)	0.009	0.456	0.629	0.679	0.684	0.705	99.98	0/17	14h06
IMP(iter #2)	0.008	0.446	0.624	0.646	0.68	0.700	99.98	0/17	21h09
IMP(iter #3)	0.009	0.454	0.638	0.655	0.676	0.689	100	0/17	28h12
IMP(iter #4)	0.007	0.478	0.641	0.658	0.677	0.687	99.95	0/17	35h15
IMP(iter #5)	0.010	0.507	0.658	0.659	0.698	0.702	99.96	0/17	42h18
IMP(iter #6)	0.006	0.530	0.577	0.676	0.688	0.691	100	0/17	49h21
IMP(iter #7)	0.003	0.488	0.495	0.518	0.629	0.657	99.95	0/17	56h26
NEPENTHE(iter #1)	0.001	0.512	0.551	0.649	0.686	0.702	99.98	0/17	14h19
NEPENTHE(iter #2)	0	0	0.001	0.031	0.453	0.460	99.93	2/17	21h35
NEPENTHE(iter #3)	0	0	0.012	0.397	0.440	0.598	99.91	2/17	28h51
NEPENTHE(iter #4)	0	0	0	0.006	0.013	0.371	99.86	3/17	36h07
NEPENTHE(iter #5)	0	0	0	0.001	0.005	0.054	99.84	3/17	43h23
NEPENTHE(iter #6)	0	0	0	0	0	0	99.61	8/17	50h44
NEPENTHE(iter #7)	0	0	0	0	0	0	98.75	8/17	57h57

Table 38: Test performance (top-1), bottom six layer’s entropies $\widehat{\mathcal{H}}$ and the number of removed layers (Rem.) for Swin-T on SVIRO.

Approach	$\widehat{\mathcal{H}}_1$	$\widehat{\mathcal{H}}_2$	$\widehat{\mathcal{H}}_3$	$\widehat{\mathcal{H}}_4$	$\widehat{\mathcal{H}}_5$	$\widehat{\mathcal{H}}_6$	top-1	Rem.	Time
Dense model	0.061	0.205	0.280	0.290	0.321	0.325	99.95	0/12	5h38
IMP(iter #1)	0.046	0.232	0.284	0.285	0.291	0.303	99.84	0/12	12h17
IMP(iter #2)	0.026	0.125	0.273	0.280	0.283	0.289	99.77	0/12	18h56
IMP(iter #3)	0.022	0.062	0.216	0.233	0.238	0.275	99.84	0/12	25h55
IMP(iter #4)	0.027	0.071	0.163	0.183	0.187	0.187	99.68	0/12	32h14
IMP(iter #5)	0.034	0.095	0.101	0.115	0.143	0.149	99.68	0/12	39h33
IMP(iter #6)	0.036	0.047	0.090	0.125	0.127	0.129	99.79	0/12	46h12
IMP(iter #7)	0.026	0.041	0.074	0.124	0.127	0.137	99.75	0/12	52h01
NEPENTHE(iter #1)	0.001	0.269	0.321	0.326	0.343	0.348	99.93	0/12	12h28
NEPENTHE(iter #2)	0	0.338	0.347	0.357	0.362	0.367	99.82	1/12	19h18
NEPENTHE(iter #3)	0	0.156	0.282	0.309	0.376	0.381	99.79	1/12	26h28
NEPENTHE(iter #4)	0	0.001	0.092	0.235	0.267	0.356	99.68	1/12	32h58
NEPENTHE(iter #5)	0	0	0.001	0.001	0.001	0.339	99.77	2/12	40h28
NEPENTHE(iter #6)	0	0	0	0	0	0.162	99.75	5/12	47h18
NEPENTHE(iter #7)	0	0	0	0	0	0.001	99.70	5/12	53h18

Table 39: Test performance (top-1), bottom six layer’s entropies $\widehat{\mathcal{H}}$ and the number of removed layers (Rem.) for MobileNetv2 on SVIRO.

Approach	$\widehat{\mathcal{H}}_1$	$\widehat{\mathcal{H}}_2$	$\widehat{\mathcal{H}}_3$	$\widehat{\mathcal{H}}_4$	$\widehat{\mathcal{H}}_5$	$\widehat{\mathcal{H}}_6$	top-1	Rem.	Time
Dense model	0.187	0.241	0.337	0.341	0.484	0.508	99.98	0/35	5h35
IMP(iter #1)	0.165	0.218	0.248	0.366	0.478	0.515	99.98	0/35	12h11
IMP(iter #2)	0.152	0.191	0.232	0.402	0.471	0.560	100	0/35	18h47
IMP(iter #3)	0.161	0.180	0.290	0.411	0.483	0.521	99.98	0/35	24h23
IMP(iter #4)	0.169	0.215	0.296	0.419	0.430	0.483	99.96	0/35	30h19
IMP(iter #5)	0.162	0.173	0.306	0.372	0.417	0.435	99.93	0/35	36h35
IMP(iter #6)	0.155	0.196	0.333	0.337	0.362	0.417	99.93	0/35	42h31
IMP(iter #7)	0.146	0.185	0.291	0.317	0.322	0.381	99.95	0/35	48h47
NEPENTHE(iter #1)	0.001	0.168	0.220	0.385	0.459	0.508	100	0/35	12h22
NEPENTHE(iter #2)	0.001	0.001	0.163	0.196	0.321	0.367	99.98	0/35	19h09
NEPENTHE(iter #3)	0	0	0.002	0.059	0.218	0.375	99.98	2/35	24h56
NEPENTHE(iter #4)	0	0	0.004	0.020	0.268	0.392	99.95	2/35	30h54
NEPENTHE(iter #5)	0	0	0.001	0.045	0.262	0.388	99.97	2/35	37h19
NEPENTHE(iter #6)	0	0	0	0	0.020	0.147	35.55	4/35	49h53

Table 40: Test performance (top-1), bottom six layer’s entropies $\widehat{\mathcal{H}}$ and the number of removed layers (Rem.) for BERT on QNLI.

Approach	$\widehat{\mathcal{H}}_1$	$\widehat{\mathcal{H}}_2$	$\widehat{\mathcal{H}}_3$	$\widehat{\mathcal{H}}_4$	$\widehat{\mathcal{H}}_5$	$\widehat{\mathcal{H}}_6$	top-1	Rem.	Time
Dense model	0.173	0.191	0.212	0.219	0.223	0.227	90.48	0/12	0h34
IMP(iter #1)	0.179	0.198	0.224	0.229	0.238	0.248	89.60	0/12	1h11
IMP(iter #2)	0.202	0.209	0.213	0.220	0.224	0.258	89.91	0/12	1h47
IMP(iter #3)	0.215	0.217	0.234	0.243	0.250	0.269	89.80	0/12	2h23
IMP(iter #4)	0.231	0.235	0.251	0.252	0.269	0.300	89.75	0/12	2h59
IMP(iter #5)	0.238	0.241	0.248	0.256	0.284	0.306	89.38	0/12	3h35
IMP(iter #6)	0.265	0.268	0.269	0.280	0.294	0.335	89.15	0/12	4h11
IMP(iter #7)	0.273	0.274	0.280	0.283	0.291	0.356	88.41	0/12	4h47
NEPENTHE(iter #1)	0	0	0.218	0.234	0.240	0.244	89.58	2/12	1h23
NEPENTHE(iter #2)	0	0	0.215	0.246	0.251	0.264	89.46	2/12	2h11
NEPENTHE(iter #3)	0	0	0	0.227	0.239	0.246	88.89	3/12	2h59
NEPENTHE(iter #4)	0	0	0	0.239	0.248	0.252	88.94	3/12	3h47
NEPENTHE(iter #5)	0	0	0	0.192	0.263	0.279	89.38	3/12	4h35
NEPENTHE(iter #6)	0	0	0	0	0.280	0.299	88.21	3/12	5h23
NEPENTHE(iter #7)	0	0	0	0	0.251	0.314	88.69	4/12	6h11

Table 41: Test performance (top-1), bottom six layer’s entropies $\hat{\mathcal{H}}$ and the number of removed layers (Rem.) for RoBERTa on QNLI.

Approach	$\hat{\mathcal{H}}_1$	$\hat{\mathcal{H}}_2$	$\hat{\mathcal{H}}_3$	$\hat{\mathcal{H}}_4$	$\hat{\mathcal{H}}_5$	$\hat{\mathcal{H}}_6$	top-1	Rem.	Time
Dense model	0.190	0.201	0.210	0.235	0.275	0.303	92.18	0/12	0h35
IMP(iter #1)	0.198	0.214	0.215	0.260	0.271	0.276	92.07	0/12	1h10
IMP(iter #2)	0.205	0.212	0.255	0.263	0.300	0.325	92.07	0/12	1h45
IMP(iter #3)	0.216	0.223	0.265	0.266	0.325	0.334	91.56	0/12	2h21
IMP(iter #4)	0.227	0.234	0.265	0.278	0.343	0.383	91.65	0/12	2h56
IMP(iter #5)	0.227	0.255	0.268	0.321	0.379	0.380	91.51	0/12	3h31
IMP(iter #6)	0.239	0.259	0.261	0.313	0.368	0.386	90.19	0/12	4h06
IMP(iter #7)	0.248	0.254	0.300	0.346	0.393	0.420	90.08	0/12	4h41
NEPENTHE(iter #1)	0.001	0.001	0.230	0.274	0.426	0.475	88.36	0/12	1h22
NEPENTHE(iter #2)	0	0	0.001	0.028	0.031	0.487	87.41	2/12	2h09
NEPENTHE(iter #3)	0	0	0.001	0.001	0.003	0.322	86.43	2/12	2h56
NEPENTHE(iter #4)	0	0	0	0.001	0.001	0.023	87.26	3/12	3h43
NEPENTHE(iter #5)	0	0	0	0.000	0.001	0.017	86.03	3/12	4h30
NEPENTHE(iter #6)	0	0	0	0.001	0.001	0.006	85.21	3/12	5h17
NEPENTHE(iter #7)	0	0	0	0	0	0	84.37	6/12	6h04

Table 42: Test performance (top-1), bottom six layer’s entropies $\hat{\mathcal{H}}$ and the number of removed layers (Rem.) for BERT on RTE.

Approach	$\hat{\mathcal{H}}_1$	$\hat{\mathcal{H}}_2$	$\hat{\mathcal{H}}_3$	$\hat{\mathcal{H}}_4$	$\hat{\mathcal{H}}_5$	$\hat{\mathcal{H}}_6$	top-1	Rem.	Time
Dense model	0.211	0.216	0.233	0.242	0.252	0.261	61.01	0/12	0h02
IMP(iter #1)	0.224	0.225	0.237	0.250	0.260	0.276	55.60	0/12	0h03
IMP(iter #2)	0.243	0.244	0.245	0.274	0.288	0.294	62.09	0/12	0h04
IMP(iter #3)	0.258	0.263	0.279	0.286	0.309	0.344	59.21	0/12	0h05
IMP(iter #4)	0.275	0.282	0.321	0.326	0.342	0.386	58.84	0/12	0h06
IMP(iter #5)	0.287	0.293	0.328	0.366	0.369	0.397	58.48	0/12	0h07
IMP(iter #6)	0.303	0.313	0.342	0.388	0.403	0.409	59.21	0/12	0h08
IMP(iter #7)	0.335	0.343	0.370	0.374	0.432	0.451	57.76	0/12	0h09
NEPENTHE(iter #1)	0.204	0.223	0.230	0.233	0.244	0.260	57.04	0/12	0h03
NEPENTHE(iter #2)	0.001	0.153	0.173	0.181	0.264	0.280	52.71	0/12	0h04
NEPENTHE(iter #3)	0	0.001	0.201	0.283	0.298	0.311	54.87	1/12	0h05
NEPENTHE(iter #4)	0	0	0	0.246	0.258	0.266	53.43	3/12	0h06
NEPENTHE(iter #5)	0	0	0	0.007	0.287	0.296	56.32	3/12	0h07
NEPENTHE(iter #6)	0	0	0	0.022	0.296	0.309	54.87	3/12	0h08
NEPENTHE(iter #7)	0	0	0	0.008	0.327	0.339	53.79	3/12	0h09

Table 43: Test performance (top-1), bottom six layer’s entropies $\widehat{\mathcal{H}}$ and the number of removed layers (Rem.) for RoBERTa on RTE.

Approach	$\widehat{\mathcal{H}}_1$	$\widehat{\mathcal{H}}_2$	$\widehat{\mathcal{H}}_3$	$\widehat{\mathcal{H}}_4$	$\widehat{\mathcal{H}}_5$	$\widehat{\mathcal{H}}_6$	top-1	Rem.	Time
Dense model	0.236	0.242	0.263	0.292	0.302	0.303	66,787	0/12	0h02
IMP(iter #1)	0.241	0.243	0.282	0.296	0.314	0.321	72.56	0/12	0h03
IMP(iter #2)	0.253	0.256	0.296	0.341	0.352	0.385	72.92	0/12	0h04
IMP(iter #3)	0.249	0.293	0.304	0.376	0.401	0.409	66.06	0/12	0h05
IMP(iter #4)	0.254	0.291	0.326	0.387	0.434	0.435	67.51	0/12	0h06
IMP(iter #5)	0.262	0.291	0.363	0.418	0.459	0.484	63.54	0/12	0h07
IMP(iter #6)	0.285	0.296	0.385	0.426	0.465	0.497	64.98	0/12	0h08
IMP(iter #7)	0.297	0.305	0.405	0.445	0.492	0.502	60.29	0/12	0h09
NEPENTHE(iter #1)	0.001	0.252	0.263	0.298	0.310	0.325	64.26	0/12	0h03
NEPENTHE(iter #2)	0.001	0.271	0.295	0.322	0.347	0.351	68.23	0/12	0h04
NEPENTHE(iter #3)	0	0.001	0.265	0.295	0.363	0.380	66.06	1/12	0h05
NEPENTHE(iter #4)	0	0	0.326	0.333	0.344	0.349	54.15	2/12	0h06
NEPENTHE(iter #5)	0	0	0.263	0.359	0.392	0.399	59.93	2/12	0h07
NEPENTHE(iter #6)	0	0	0.001	0.001	0.325	0.387	54.15	2/12	0h08
NEPENTHE(iter #7)	0	0	0.001	0.001	0.001	0.390	59.21	2/12	0h09

Table 44: Test performance (top-1), bottom six layer’s entropies $\widehat{\mathcal{H}}$ and the number of removed layers (Rem.) for BERT on SST-2.

Approach	$\widehat{\mathcal{H}}_1$	$\widehat{\mathcal{H}}_2$	$\widehat{\mathcal{H}}_3$	$\widehat{\mathcal{H}}_4$	$\widehat{\mathcal{H}}_5$	$\widehat{\mathcal{H}}_6$	top-1	Rem.	Time
Dense model	0.114	0.122	0.130	0.172	0.178	0.205	92,20	0/12	0h21
IMP(iter #1)	0.119	0.126	0.139	0.190	0.213	0.226	91.63	0/12	0h41
IMP(iter #2)	0.138	0.141	0.161	0.241	0.264	0.267	90.83	0/12	1h01
IMP(iter #3)	0.133	0.144	0.185	0.239	0.280	0.307	90.48	0/12	1h22
IMP(iter #4)	0.142	0.167	0.205	0.251	0.303	0.332	90.37	0/12	1h43
IMP(iter #5)	0.158	0.181	0.219	0.279	0.312	0.376	89.91	0/12	2h04
IMP(iter #6)	0.178	0.215	0.241	0.322	0.361	0.363	88.53	0/12	2h25
IMP(iter #7)	0.187	0.226	0.270	0.365	0.370	0.466	87.96	0/12	2h46
NEPENTHE(iter #1)	0.001	0.132	0.137	0.182	0.224	0.229	91.17	0/12	0h48
NEPENTHE(iter #2)	0.001	0.001	0.191	0.209	0.238	0.246	89.68	0/12	1h16
NEPENTHE(iter #3)	0	0	0	0.193	0.205	0.224	89.00	3/12	1h44
NEPENTHE(iter #4)	0	0	0	0.001	0.204	0.243	88.88	3/12	2h12
NEPENTHE(iter #5)	0	0	0	0.001	0.228	0.254	87.39	3/12	3h01
NEPENTHE(iter #6)	0	0	0	0.001	0.246	0.252	88.76	3/12	3h29
NEPENTHE(iter #7)	0	0	0	0.001	0.245	0.253	87.73	3/12	3h57

Table 45: Test performance (top-1), bottom six layer’s entropies $\hat{\mathcal{H}}$ and the number of removed layers (Rem.) for RoBERTa on SST-2.

Approach	$\hat{\mathcal{H}}_1$	$\hat{\mathcal{H}}_2$	$\hat{\mathcal{H}}_3$	$\hat{\mathcal{H}}_4$	$\hat{\mathcal{H}}_5$	$\hat{\mathcal{H}}_6$	top-1	Rem.	Time
Dense model	0.131	0.145	0.152	0.187	0.192	0.278	92.66	0/12	0h21
IMP(iter #1)	0.129	0.151	0.153	0.189	0.196	0.276	92.32	0/12	0h41
IMP(iter #2)	0.136	0.155	0.156	0.186	0.226	0.266	92.43	0/12	1h01
IMP(iter #3)	0.159	0.173	0.179	0.195	0.234	0.346	93.23	0/12	1h22
IMP(iter #4)	0.178	0.180	0.215	0.227	0.304	0.374	92.66	0/12	1h43
IMP(iter #5)	0.178	0.199	0.253	0.293	0.319	0.419	92.20	0/12	2h04
IMP(iter #6)	0.177	0.208	0.226	0.280	0.323	0.416	91.17	0/12	2h25
IMP(iter #7)	0.174	0.200	0.220	0.285	0.344	0.428	90.83	0/12	2h46
NEPENTHE(iter #1)	0.001	0.128	0.160	0.161	0.202	0.255	92.32	0/12	0h48
NEPENTHE(iter #2)	0.001	0.001	0.166	0.205	0.216	0.251	92.09	0/12	1h16
NEPENTHE(iter #3)	0	0.001	0.162	0.197	0.283	0.322	90.83	1/12	1h44
NEPENTHE(iter #4)	0	0	0.191	0.198	0.257	0.267	90.60	2/12	2h12
NEPENTHE(iter #5)	0	0	0.191	0.212	0.281	0.345	90.48	2/12	3h01
NEPENTHE(iter #6)	0	0	0.001	0.210	0.293	0.378	90.71	2/12	3h29
NEPENTHE(iter #7)	0	0	0.001	0.215	0.272	0.275	89.68	2/12	3h57

D.5 Practical Sanity Checks on Gaussian Assumptions

Our derivation is based on the assumption that the weights of a layer and the inputs for its corresponding rectifier activation are Gaussian distributed. We validate here this assumption empirically. Fig. 7, 9, 11, 13, 15 show the weights distribution for each rectifier activated layer for all the models employed in our experiments. Moreover, Fig. 8, 10, 12, 14, 16 show the input distribution for each rectifier layer for each model used in our experiments. Inputs from CIFAR-10 are used for ResNet-18, Swin-T, and MobileNet-V2 models, while inputs from QNLI are employed for BERT and RoBERTa models. It appears that the weights and the inputs of the corresponding layers are following a Gaussian distribution.

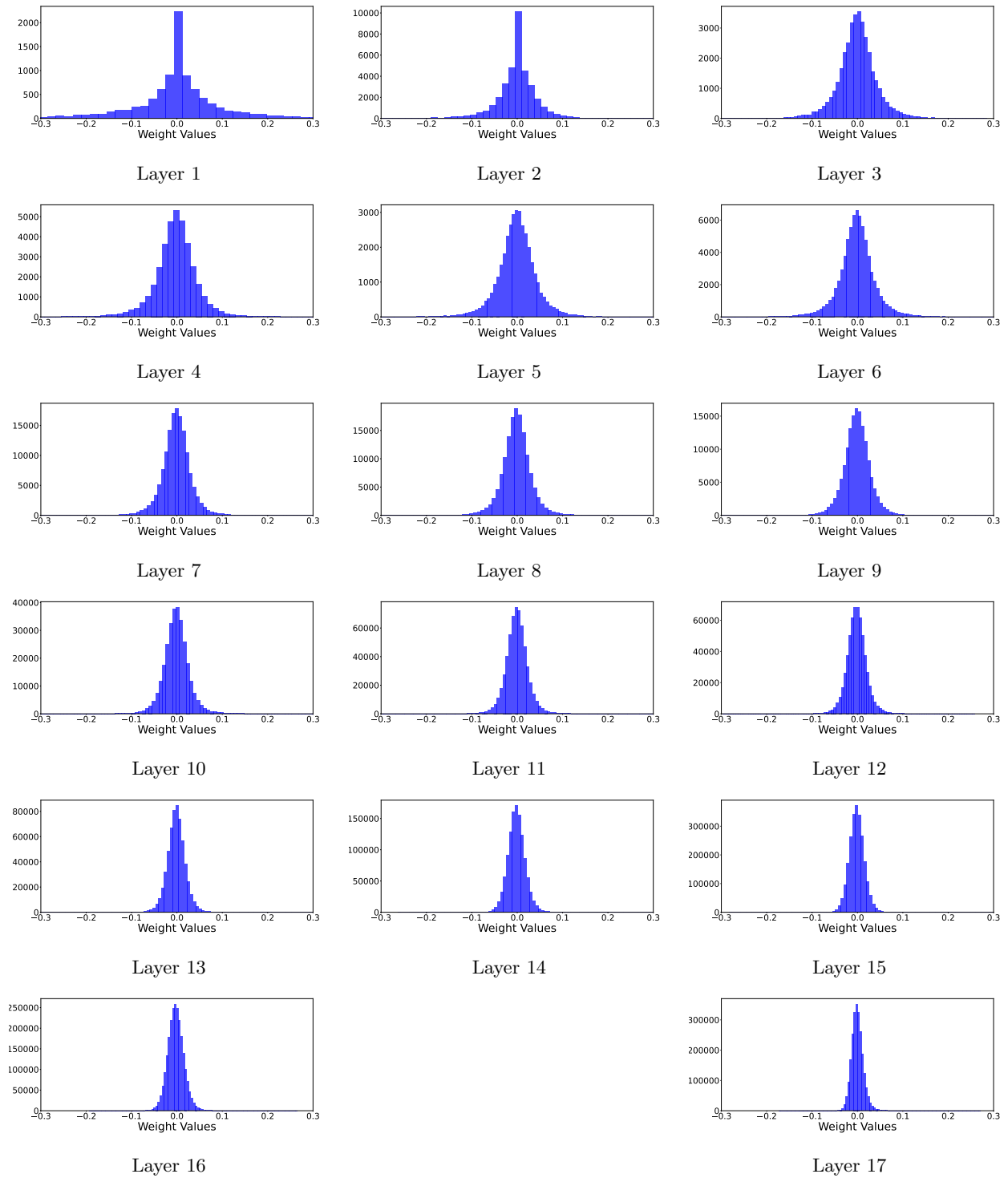


Figure 7: Weights distribution of each layer in ResNet-18.

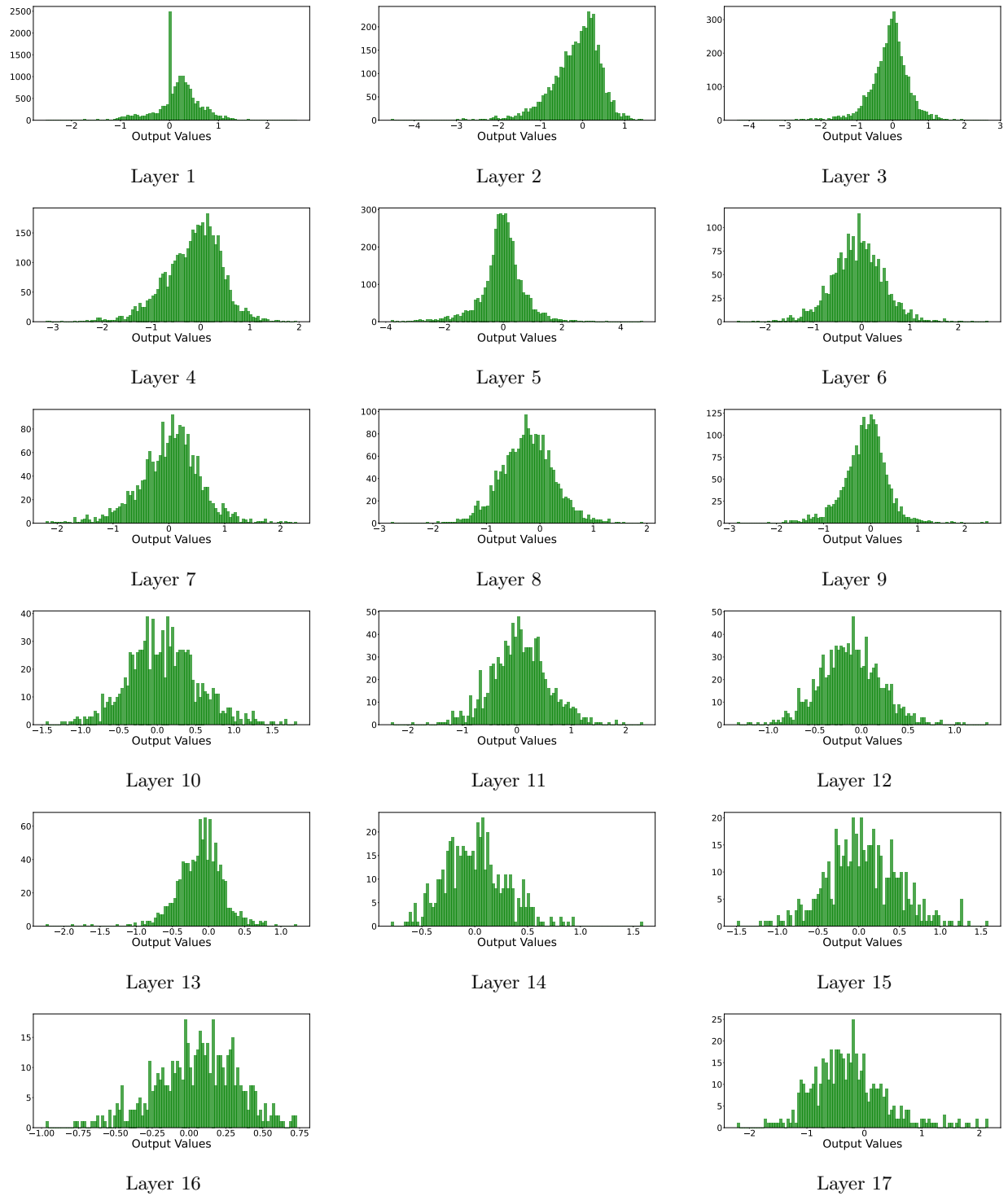


Figure 8: Input distribution of each layer in ResNet-18.

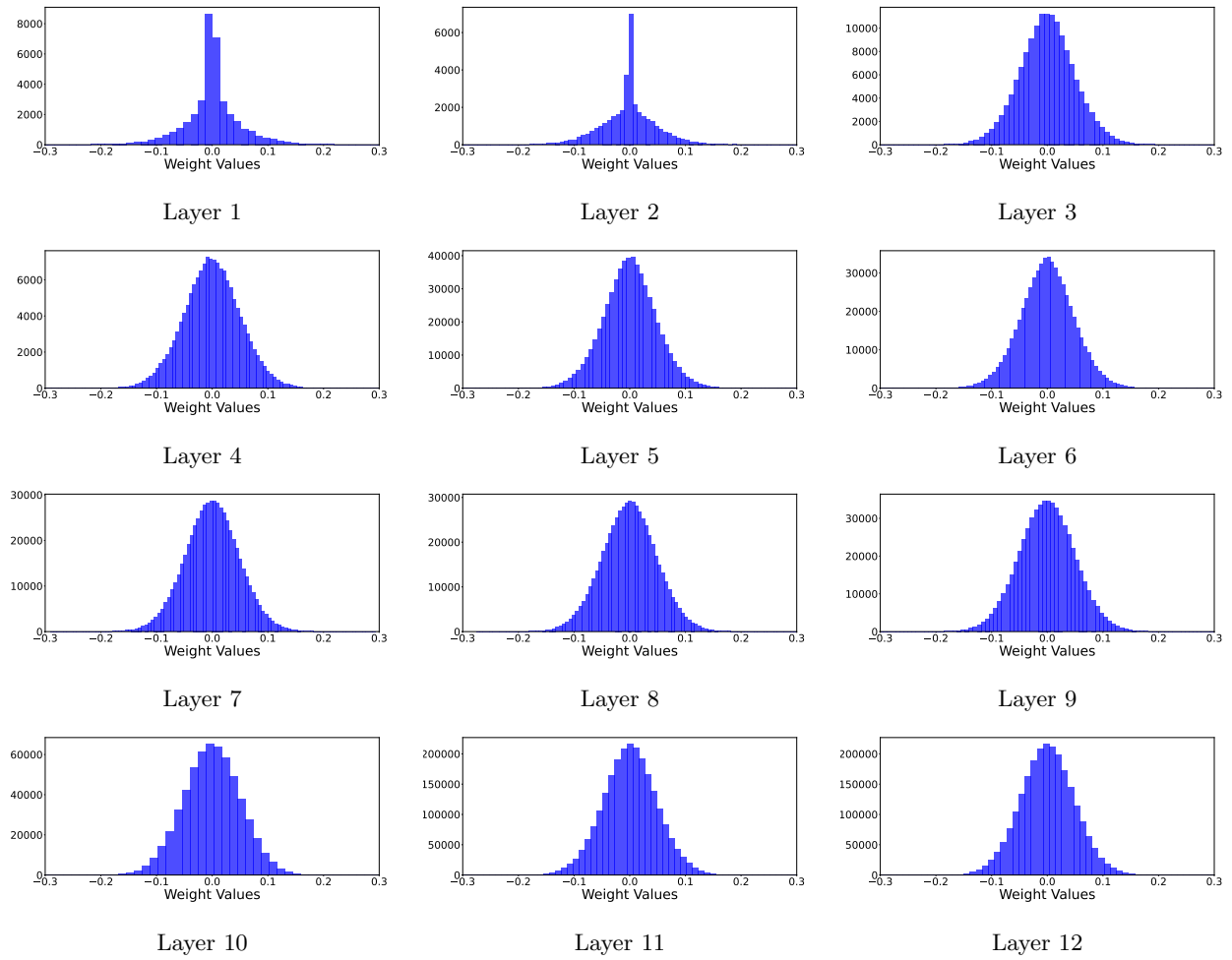


Figure 9: Weights distribution of each layer in Swin-T.

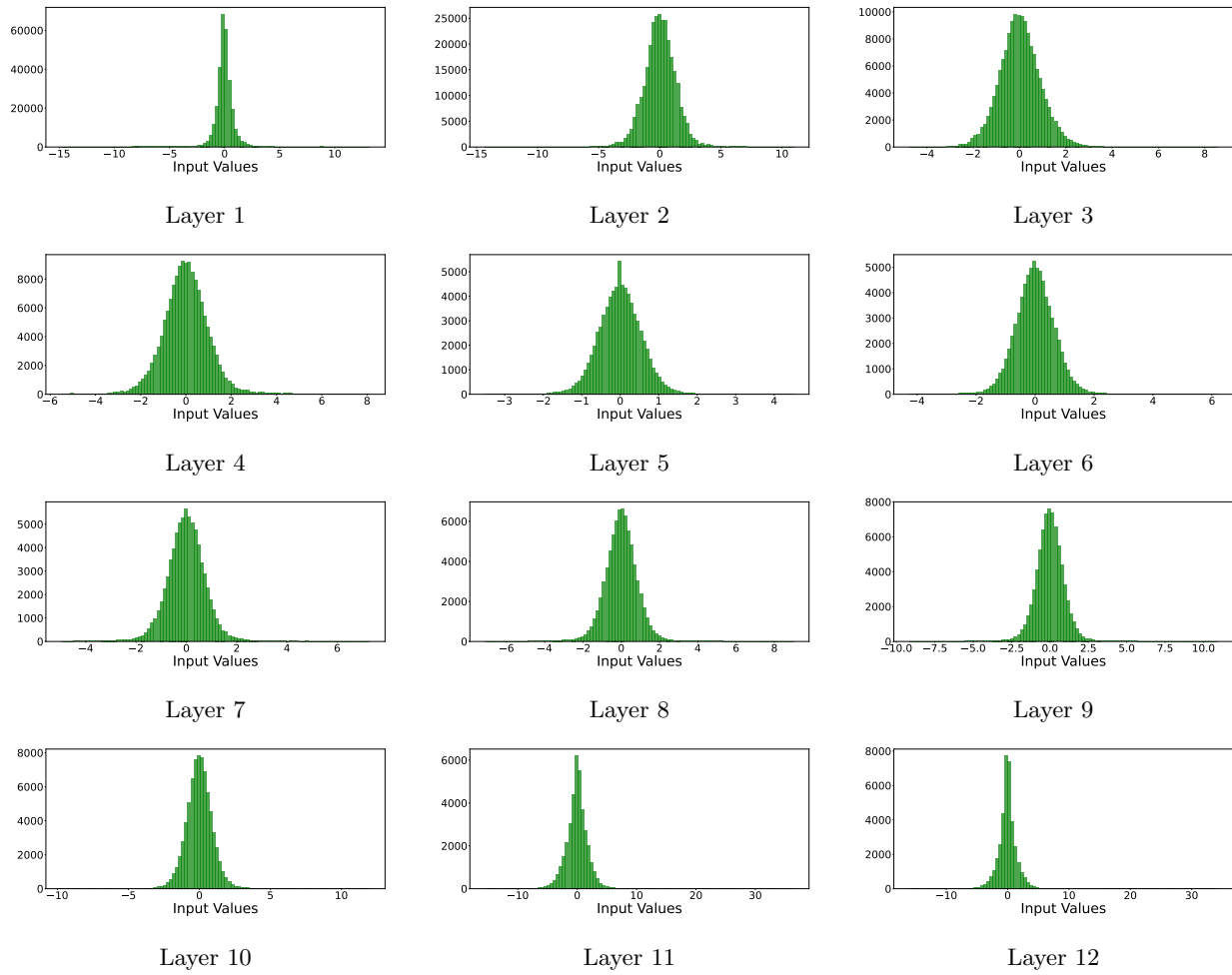


Figure 10: Input distribution of each layer in Swin-T.

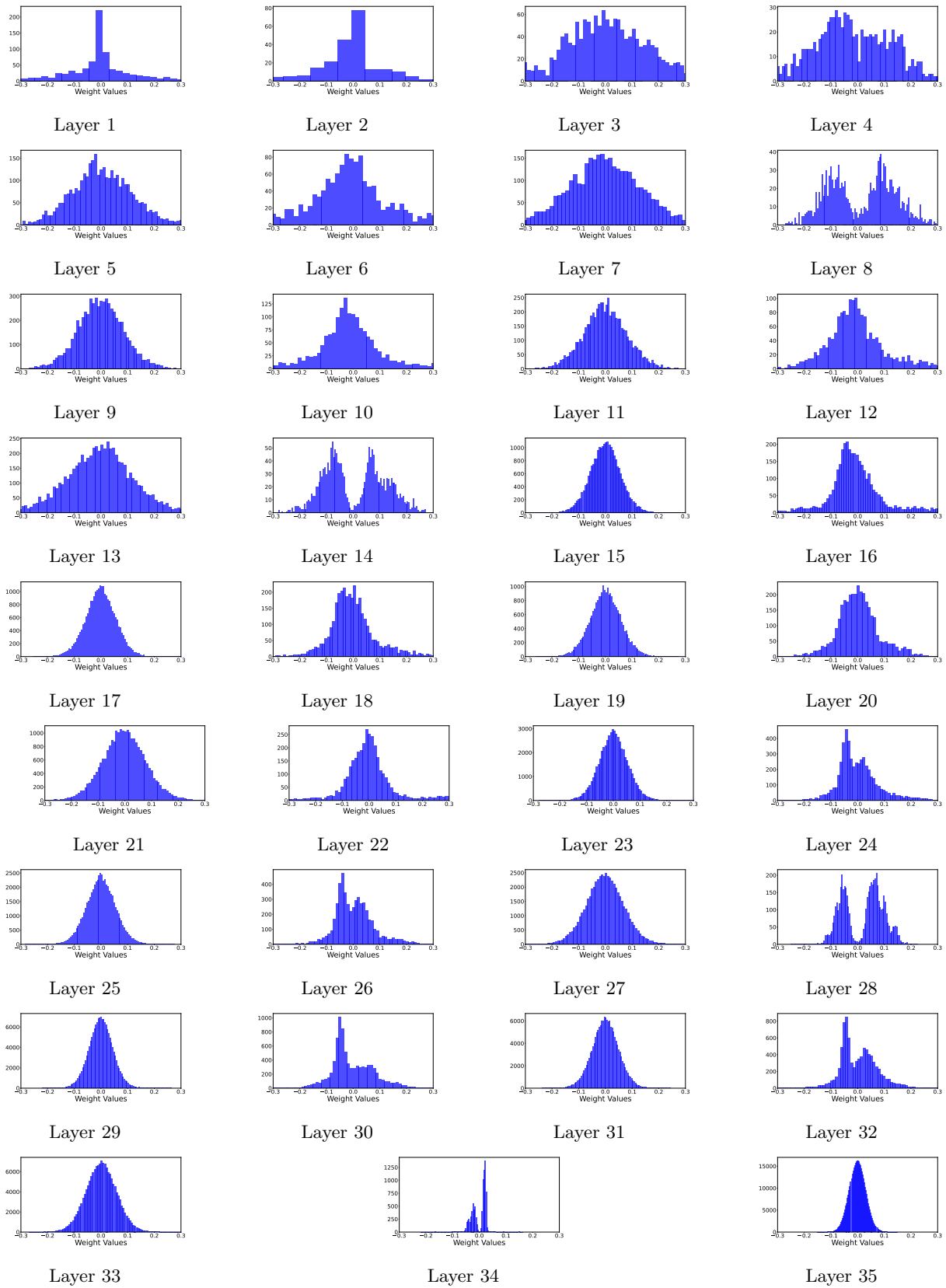


Figure 11: Weights distribution of each layer in MobileNet.

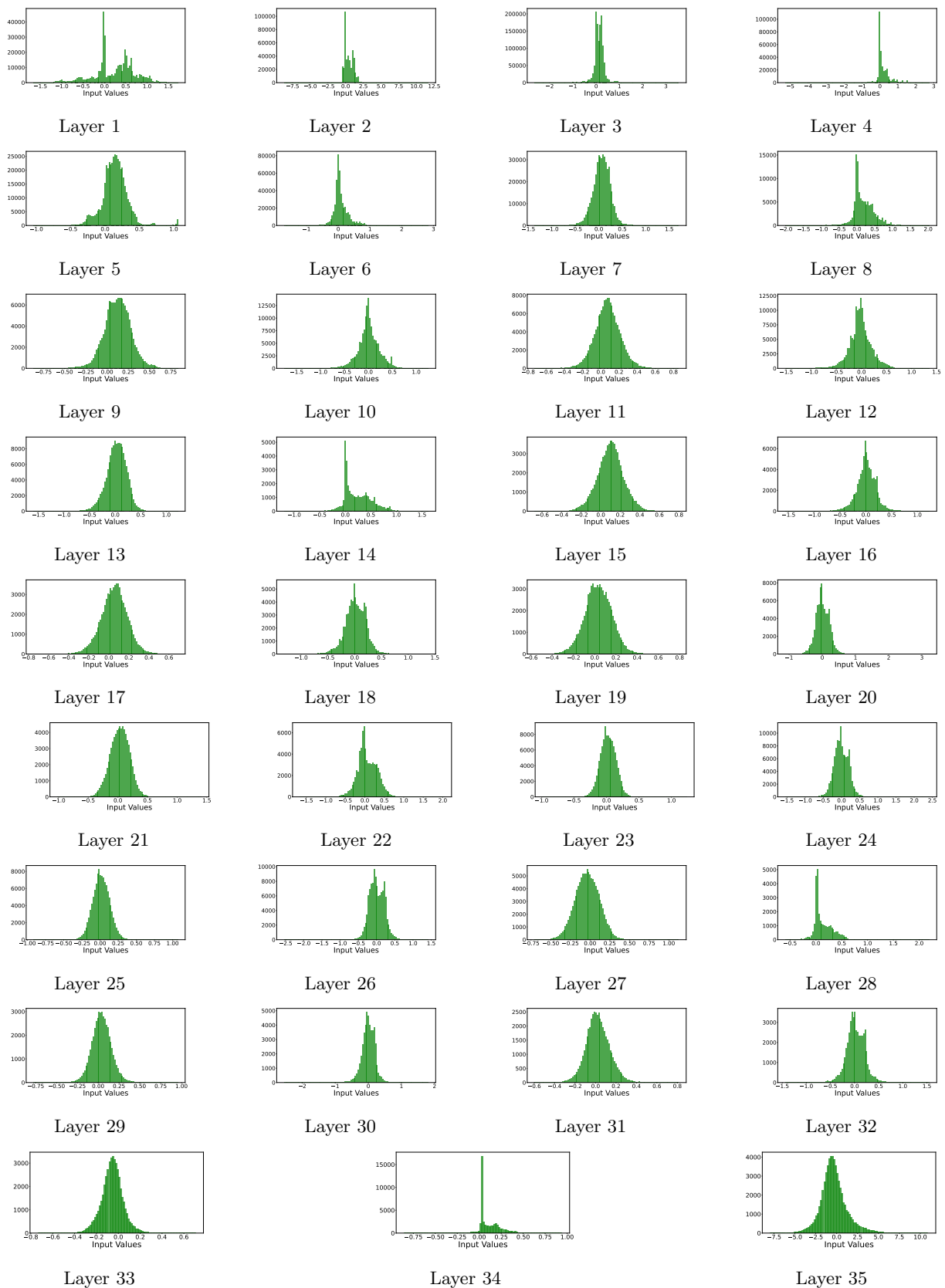


Figure 12: Input distribution of each layer in MobileNet.

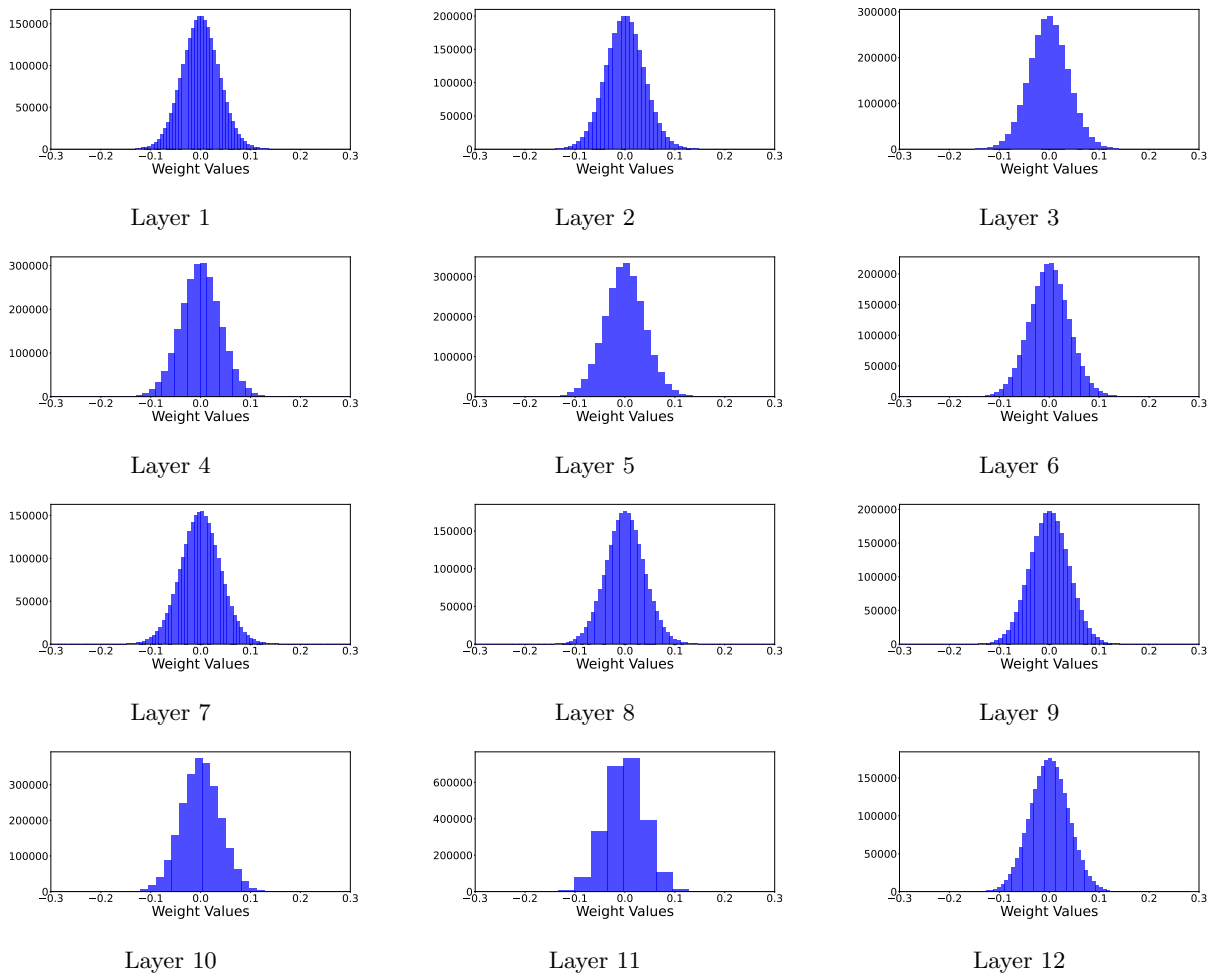


Figure 13: Weights distribution of each layer in BERT.

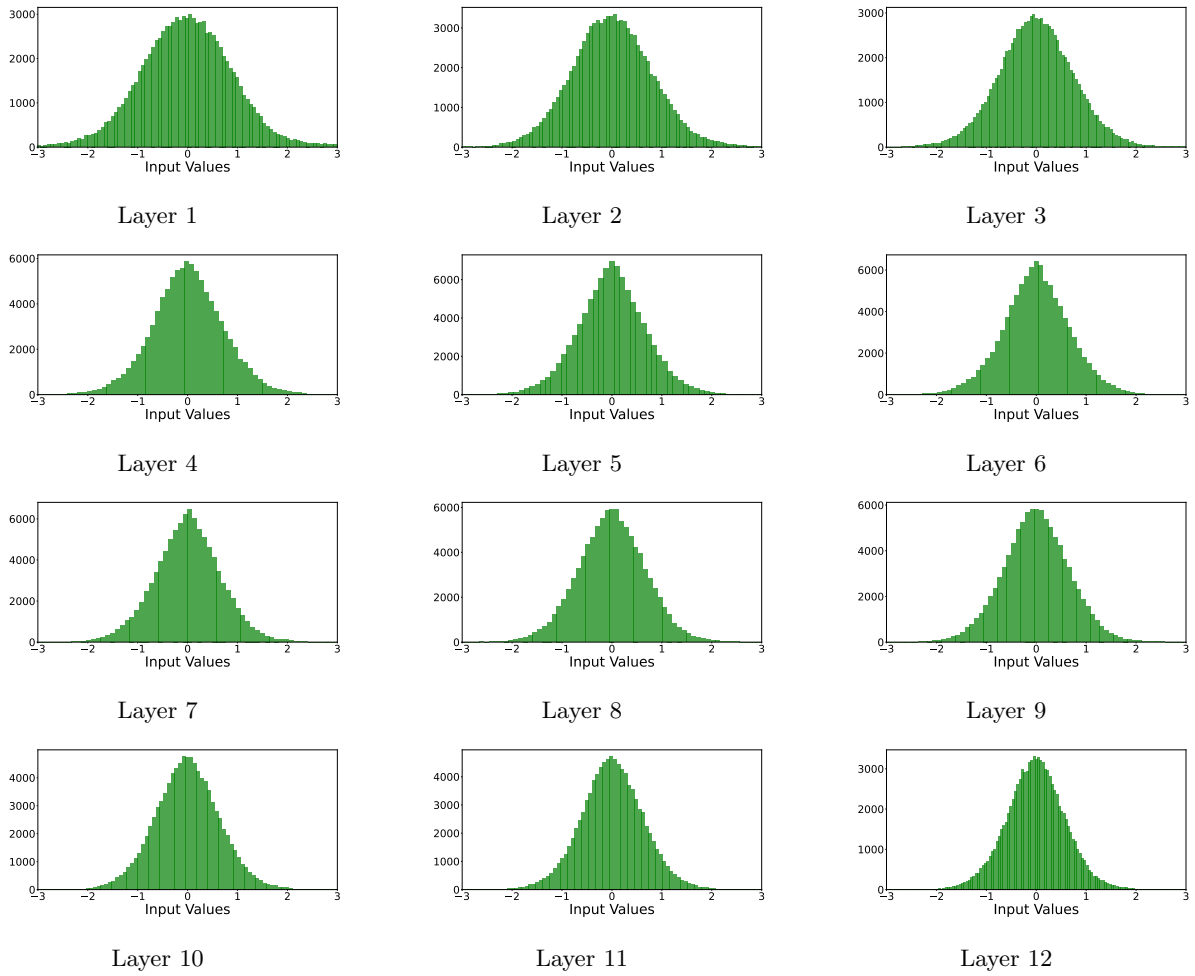


Figure 14: Input distribution of each layer in BERT.

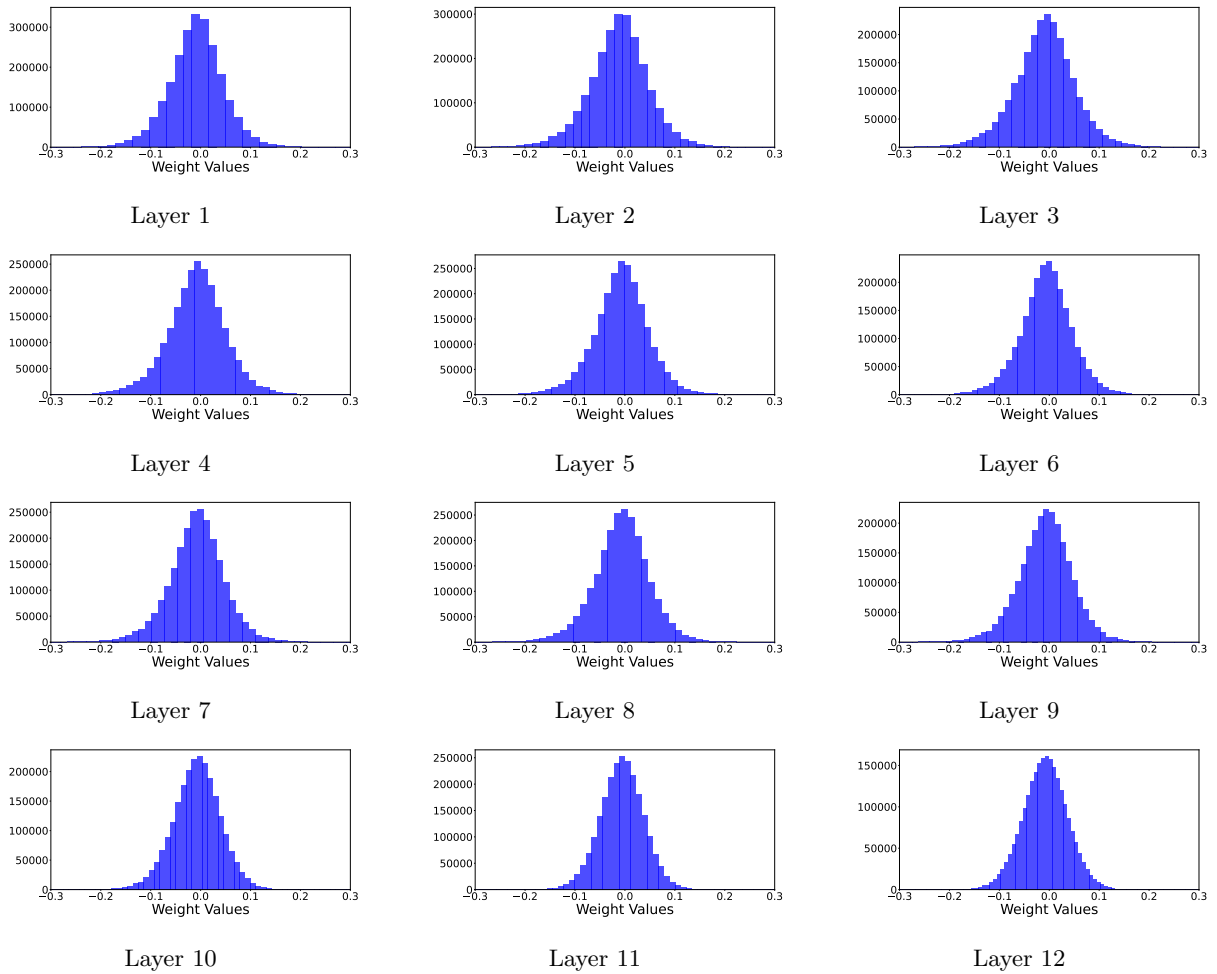


Figure 15: Weights distribution of each layer in RoBERTa.

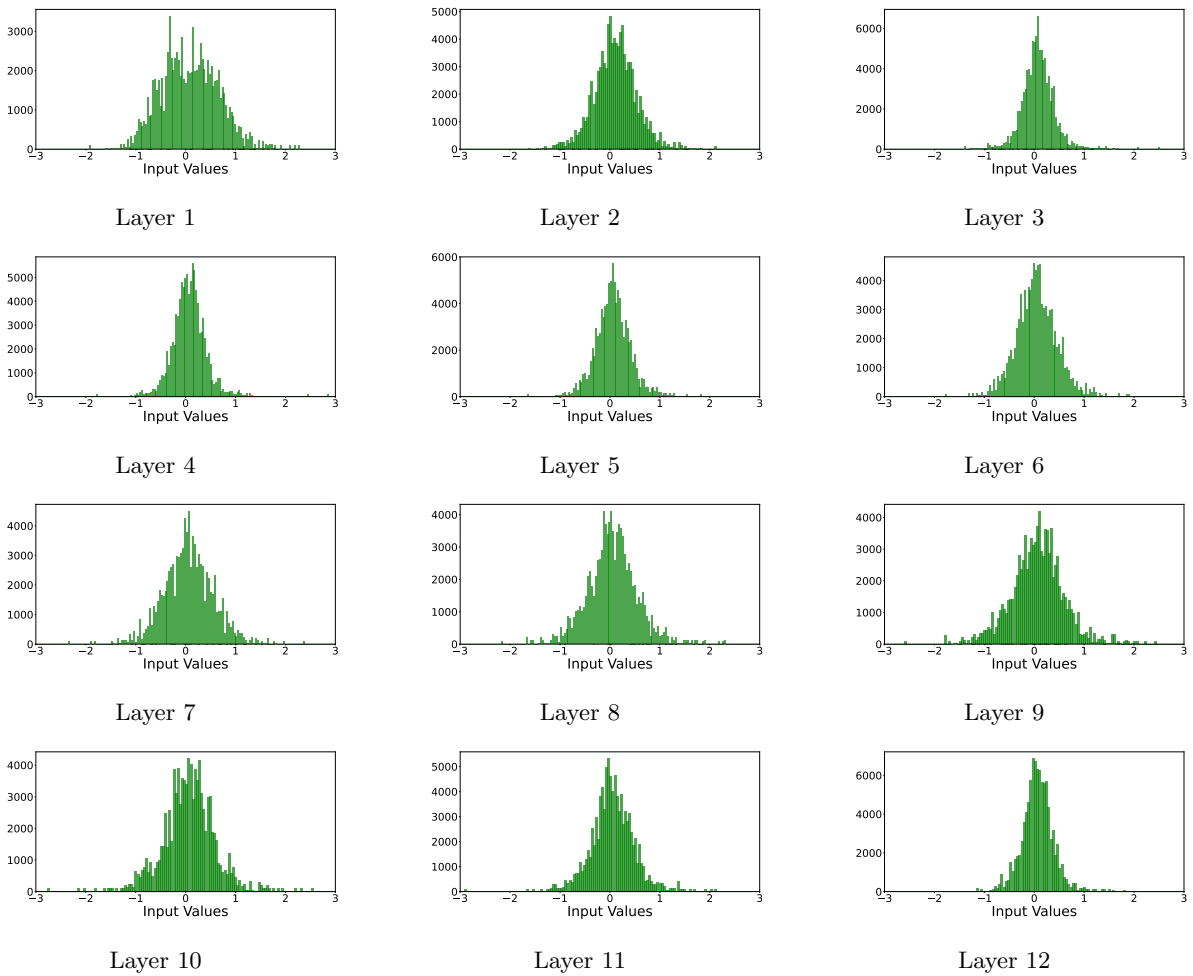


Figure 16: Input distribution of each layer in RoBERTa.